Beyond 5G White Paper
Supplementary Volume
“Relay and Reflector Technologies”

Version 1.0

March 7, 2024

XG Mobile Promotion Forum

【Revision History】

Ver.	Date	Contents	Note
1.0	2024.3.7	Initial version	

Preface

In our published white paper “Beyond 5G White Paper ~Message to the 2030s~”, we researched what are required in various industries in the Beyond 5G era, then we proposed “Further enhancement of specific 5G features” such as ultra-high speed wireless communications of 10 times faster than that of 5G, 100 times capacity larger than 5G, and 1/100th of 5G’s power consumption. To address these targets, we need possibility of relay and reflector technologies to realize New Radio Network Topology (NRNT) as one of key Beyond 5G technologies.

For pursuing ultra-high speed and large capacity (especially uplink) wireless communications with improved reliability, it is ideal to communicate in a shorter distance with a LOS (Line of Sight) environment (in a path with a smaller radio propagation loss) and increase the number of paths for the wireless communications to provide more options (more redundancy) as much as possible. Satisfying these conditions will require a network topology distributed in the space domain. Early generations of mobile communication systems considered it ideal to configure a cellular network with hexagonal cells to avoid inter-cell interference. In the Beyond 5G era, however, there will be an evolution to NRNT. This new form of radio access network will be a further extension of a heterogeneous network which has been studied since 4G, with overlapping multiple cell areas for creating more LOS environments and path options, and with more connection routes to/from mobile terminals nearby as well as other networks including Non-Terrestrial Network (NTN).

Such a spatially distributed network is considered to be compatible with high frequency bands such as millimeter wave and sub-Terahertz bands, cell-free/distributed MIMO, wireless sensing, and wireless power supply. On the other hand, from a common-sense viewpoint, the NRNT may not be an ideal network configuration as it generates inter-cell interference and has many redundant base station antennas. This topology is not immune to interference because it does not adopt advanced beam control or path selection, or a cell configuration where each antenna forms a zone to avoid interference. Hence, a technical solution is required to help prevent interference, such as a cell-free MIMO configuration, which configures a cell by multiple base station antennas.

How to economically realize the NRNT is also a fundamental problem, and we can think of various approaches to tackle this technical issue. The standard solution would be not to use conventional base station antennas only. There are a lot of research and development activities: the use of existing objects such as streetlamps, street/traffic lights, signboards, vending machines and window glass for antennas, integration of sensors and antennas, relay such as IAB (Integrated Access and Backhaul) and repeaters, reflectors such as Reconfigurable Intelligent Surface (RIS)/Intelligent Reflecting Surface (IRS), which are installed between base stations and mobile stations, and terminal

collaboration/inter-terminal cooperation that virtually increases the number of mobile station antennas. In addition, it may be necessary to establish new wireless and optical interconnection and transmission systems which enable a distributed network topology and have a scalability to follow future evolution of the wireless communications, as well as fronthaul and backhaul (xhaul) technologies. By exploiting such new solutions in combination with existing cellular configurations, NRNT can provide stable, high-speed, and large-capacity wireless communications in addition to coverage extension regardless of users' locations.

To tackle these challenges and realize new use cases, there are a lot of research and development activities on the relay and reflector technologies in Japan. Note that cell-free/distributed MIMO is discussed in detail in our other white paper. In this white paper, these research and development activities and their results with a lot of figures are shown as follows:

- "Analysis of Using Transmissive Metasurfaces toward Beyond 5G" describes a novel solution that combines multiple transmissive metasurfaces with beamforming in a 28 GHz-band base station, and experimental results show that the solution using five transmissive metasurfaces can drastically improve downlink throughput at the foot of the building.

- "High-Performance Radio Propagation Simulation Method for Path Loss Estimation" describes a simulation technology for estimating and predicting radio propagation characteristics with short calculation time and high accuracy for maximizing performances, quality assurance, and efficient operation of the Beyond 5G system with the complex and varying radio network topology.

- "Relay-Related Technologies in New Radio Network Topology (NRNT)" describes two experimental results in indoor experimental evaluations to realize NRNT. The first experiment examines a reception power improvement achieved by developing RIS, and the second experiment assess an environmental resistance resulting from the application of network topology control, which includes the integration of relay nodes.

- "Development of Meta-surface Reflectors for Millimeter-wave Mobile Communication Systems" describes a development and characterization of meta-surface reflectors based on an optically transparent dual-band meta-surface reflector and a liquid-crystal RIS. An evaluation method for the scattering characteristics of the reflectors is also provided.

- “Terminal-Collaborated MIMO Reception” describes efficient subband-based terminal selection schemes where the collaboration terminals in terminal-collaborated MIMO reception are selected based on the MIMO channel matrices and the residual error coefficients. Simulation results show that the proposed schemes have superior transmission performance compared to the conventional schemes.

- “Beamforming-Based IRS Control for Sub-Terahertz-Band Communications in Indoor Office Environments” describes an IRS control method based on beamforming that is realized by phases of a Butler or DFT matrix. Simulation results show that the IRS control method reveals good performance in the sense that a received power is not so lower than an upper bound value.

- “Beam Squint-aware Frequency Resource Allocation for IRS-aided Communication” describes a proposed method that utilizes a beam squint to increase the frequency efficiency by optimizing the IRS reflection direction and resource allocation. Simulation results demonstrate that the proposed method is more effective in environments with dense terminals and high beam squint.

- “Prototype and Evaluation of Intelligent Reflecting Surface for 60 GHz Band” describes a design and an electromagnetic simulation model of a developed prototype IRS for 60 GHz band and the electromagnetic simulation results are shown. In addition, results of characterization experiments verify the effectiveness of the developed IRS as a device for improving the propagation path.

- “Wireless Transport Technology for Xhaul” shows basic evaluation results of a developed 60 GHz wireless transport equipment for xhaul. For its application to a mobility platform, experimental results demonstrate that the use of millimeter wave sensors to predict radio quality can avoid blocking and realize seamless radio access technology change and handover.

- “A Study on High-Capacity UL Communication in Relay Systems with UAV” describes an optimal placement method of Relay Station (RS) such as Unmanned Aerial Vehicle (UAV) considering the multiplicity of user equipment accommodations and the robust LOS-MIMO to increase uplink system capacity between RS and BS. Simulation results show the effectiveness of the proposed optimal placement method.

In conclusion, as we embark on the journey towards Beyond 5G technologies, the relay and reflector technologies emerge as one of key elements in this technological evolution. Japan's endeavor to overcome the challenges to realize the relay and reflector technologies, coupled with its commitment to research and development in this domain, positions it at the forefront of this next-generation communication revolution. This white paper aims to provide a comprehensive overview of the potential, challenges, and future directions of the relay and reflector technologies for Beyond 5G, with a particular emphasis on their initiatives and advancements in Japan.

This White Paper was prepared with the generous support of many people who participated in the White Paper Subcommittee. The cooperation of telecommunications industry players and academia experts, as well as representatives of various industries other than the communications industry has also been substantial. Thanks to everyone's participation and support, this White Paper was able to cover a lot of useful information for future business creation discussions between the industry, academia, and government, and for investigating solutions to social issues, not only in the telecommunications industry, but also across all industries. We hope that this White Paper will help Japan create a better future for society and promote significant global activities.

Satoshi Suyama
NTT DOCOMO, INC.

I. Analysis of Using Transmissive Metasurfaces toward Beyond 5G

Kenta Goto, Satoshi Suyama
NTT DOCOMO, INC.
Daisuke Kitayama
NTT Device Technology Labs., NTT Corporation.

Abstract— **Toward further enhancement of 5G and Beyond 5G/6G, metasurface and reconfigurable intelligent surface (RIS) have been attracting much attention thanks to cost-effective and energy-efficient features. Experimental trials have been conducted to verify their effectiveness. In consideration of a legacy deployment, it is difficult to create a coverage area at the foot of a building in millimeter-wave (mmW) bands. Thus, for mmW coverage enhancement, we propose a novel solution that combines multiple transmissive metasurfaces (TMSs) with beamforming (BF) in a base station (BS). To verify the effectiveness of our proposed solution, experimental trials using a 28 GHz-band 5G BS and a user equipment were conducted. The BF function selectively aims the beam at one of five TMSs, and then TMS re-directs the radio wave to the foot area. This paper introduces an overview of the trials and shows downlink throughput measured in the trials. In addition, toward 6G, novel design methodology of TMSs for sub-terahertz band and its effectiveness are introduced.**

I-1. Introduction

In order to meet various use cases for further enhancement of 5G (5G Evolution) and Beyond 5G/6G, a future radio access network that can flexibly realize a variety of higher requirements is expected to be required. In recent years, a technical concept called New Radio Network Topology (NRNT) has been proposed to improve performances of radio access technologies (RATs) by increasing the number of line-of-sight (LOS) paths between multiple base station (BS) antennas (replacements) and a target user equipment (UE) and providing more room for path selection [1].

Elemental technologies for NRNT are metasurface and reconfigurable intelligent surface (RIS). Metasurface, an artificially engineered material, is comprised of a set of periodically arranged wavelength-order-sized unit cells and is a passive device. RIS is capable of adaptively manipulating incoming radio waves by using external stimuli and is an active device. It can improve various radio access performances, and thanks to cost effective and energy efficient features, a great deal of studies have been reported in recent years [2]-[7].

In the case of service area deployment in outdoor, it is difficult to create a coverage area at the foot of a building, when a base station (BS) is installed on the rooftop of the same building. High frequency bands such as millimeter-wave (mmW) band have

significant distance attenuation and linearity, and this technical issue becomes more pronounced as the frequency is higher. To solve this problem, the authors propose a new solution that combines a beamforming (BF) function in BS with multiple transmissive metasurfaces (TMSs). In order to demonstrate the effectiveness of the proposed solution, 28 GHz-band experimental trials were conducted from October to November 2022 [8]. A 28 GHz-band 5G non-stand-alone (NSA) BS and a UE were used. BS with the BF function was deployed inside the building of DOCOMO R&D Center, and five TMSs were attached to a glass window in front of BS. This paper shows transmission performances measured by mmW experimental equipment of 5G BS and UE. Through the experimental trials, it is cleared the proposed solution can expand a mmW coverage area at the foot of the building in an indoor to outdoor scenario. Moreover, for sub-terahertz band toward 6G, we introduce our design methodology that is twisted metasurface structure and a backside polarization layer and experimentally confirm the effectiveness of this approach. The proposed structure is robust against interlayer alignment errors.

I-2. 28 GHz-Band Experimental Trials Using Transmissive Metasurface

The authors have proposed a novel cost-effective massive MIMO (mMIMO) transmitter architecture exploiting RIS for 6G in the high frequency bands, which is called RIS-aided mMIMO [5]. In RIS-aided mMIMO, a small-size phased array antenna performs the first BF, and then multiple transmissive RISs carry out the second BF to adaptively control the beam generated by the first BF. For example, the RIS-aided mMIMO using above 2-step BF procedure generates a pencil beam for long-distance transmission or orthogonalizes spatially multiplexed MIMO streams to achieve extremely high capacity for 6G. However, it is not easy to apply the proposed RIS-aided architecture to a current experimental equipment of BS. Thus, in order to evaluate the potential of the RIS-aided architecture by an experimental trial, a simplified architecture that combines the first BF procedure with multiple passive TMSs is proposed in this paper. The BF function in BS directs the beam to the multiple TMSs, allowing the radio waves through TMSs to reach UEs which are located at the foot of the building. TMSs are designed to re-direct the incident waves to the downward direction. Especially in the high frequency bands, it is inherently difficult to directly deliver the radio waves to the foot area. In addition, detailed characteristics of each TMS can designed individually, and the BF function selects the best TMS among the multiple ones based on the maximum received power criterion, when the number of beams is one (single-beam transmission) and the distance between BS and TMSs is not so long. Of course, the number of the selected TMSs strongly depends on the number of beams in BS and the distance. To demonstrate the effectiveness of the simplified architecture with BF and TMSs, the mmW experimental trials were conducted from October to November 2022 at the DOCOMO R&D Center in

Kanagawa Prefecture, Japan. Fig. I-1 shows the configuration of the experimental trials. A 5G NSA BS and a commercially available UE were used as the experimental equipment in the trials. BS was deployed inside the building of the DOCOMO R&D center with the BS antenna facing horizontally parallel to the ground surface without antenna tilt, and five TMSs were attached horizontally based on the intersection of a glass window in front of BS and the extension of the central axis of the BS antenna. The distance between BS and the window glass (TMSs) is set to 0.9 m and the BS antenna height is approximately 20 m. A trolley with UE was moved at a speed of approximately 5 km/h within the premises of the DOCOMO R&D center including the foot of the building and on the sidewalk, near the building. UE measured DL throughput. In the trials, to reduce an influence of the human shielding caused by the measurer, the trolley was always pulled in the direction away from BS. UE was oriented to match the direction of the person moving the trolly, assuming that a person was operating a smartphone. UE was also adjusted to be almost 1.2 m high by using a styrene foam, and a laptop personal computer was connected to UE for the measurement. Main specifications of the BS equipment are summarized below. The center frequency and the system bandwidth are set to 27.65 GHz, and 300 MHz, respectively. The BS antenna is mMIMO having 512 antenna elements in total, 256 elements per polarization, and it has analog BF function. It can transmit up to two streams for the MIMO spatial multiplexing. Note that the center frequency and the system bandwidth in LTE are 2667.5 MHz, and 5 MHz, respectively.

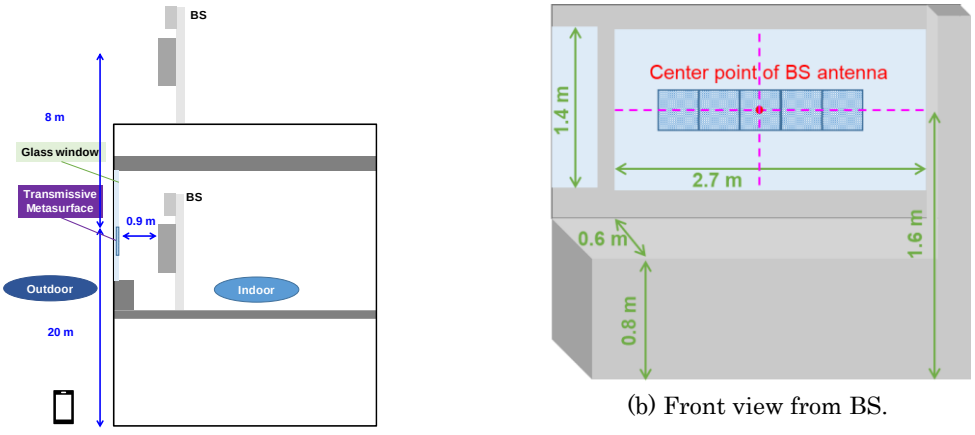

(a) Side view.

(b) Front view from BS.

Fig. I-1. Experimental environment.

I-3. Experimental Results

Let us show some experimental results measured in mmW experimental trials exploiting five TMSs. The heat maps of the DL throughput are shown in Fig. I-2. The white box in Fig. I-2 is a target area that can be expected to be improved based on the design of TMSs and is in NLOS environments. Fig. I-2 (a) show that approximately 1 Gbps maximum DL throughput can be achieved in the target area and that the DL

throughput drastically increases thanks to TMSs, compared to the result of legacy deployment shown in Fig. I-2 (b) which describes the DL throughput when BS was deployed on the rooftop of the building which is almost 28 m high. Since the trial was conducted on different dates, January 2023, the trees around the measurement area were cut down, and thus the blocking effect of the trees must be reduced. In addition, BS performances were improved by updating the software installed into BS. However, from Fig. I-2 (b), it can be seen that the measured DL throughput is only a few Mbps at the foot of the building, and that it is difficult to create 28 GHz-band coverage area at the foot of the building. Therefore, the combination of the BF function in BS and multiple TMSs is considered to be a great effective solution toward realizing the mmW coverage enhancement.

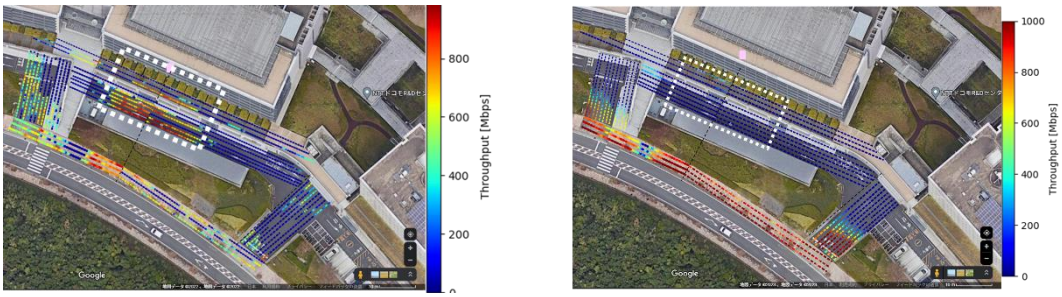

(a) With TMSs. (b) Legacy deployment (installed on the rooftop of the building).

Fig. I-2. Heatmap of DL throughput.

I-4. TMSs for Sub-terahertz Band toward Beyond 5G

As described in the previous sections, TMS is effective in optimizing millimeter-wave coverage. It can be inferred that sub-terahertz band, which are being considered for use in 6G systems, will face the same coverage challenges as millimeter-wave band. TMS becomes even more important in 6G systems because the higher the frequency, the greater the impact of TMS on the wireless environment for the same aperture size. In the previous sections, the propagation direction was determined based on the transmission intensity profile. However, to improve the aperture efficiency, it is better to determine the propagation direction based on the phase profile.

Huygens metasurfaces are promising to make transmission phase profiles with low loss because they allow for phase design in the range of 2π while still matching the free-space wave impedance. Some works have reported the implementation of this approach with two metal layers on a single substrate [6]. However, a Huygens metasurface uses both electric and magnetic resonance simultaneously to obtain the desired impedance, which requires high alignment precision between the layers. Static-type TMSs applied to window glass or walls should be inexpensive and easy to fabricate from industrial perspective.

In [7], twisted metasurface structure and a backside polarization layer are used to efficiently make a transmission phase profiles by using scattered waves of polarization orthogonal to the incident waves as transmitted waves (Fig. I-3 (a)). A 1-bit 0/π phase profile can be made with low loss of less than 1 dB by simply changing the twist direction of the structure, enabling a focusing and deflection function at 110 GHz as shown in Fig. I-3 (b). This structure is robust to interlayer alignment errors because the scattering phase is independently determined only in the metasurface layer, while the polarizer is used only to improve the efficiency, which is an advantage from a fabrication point of view.

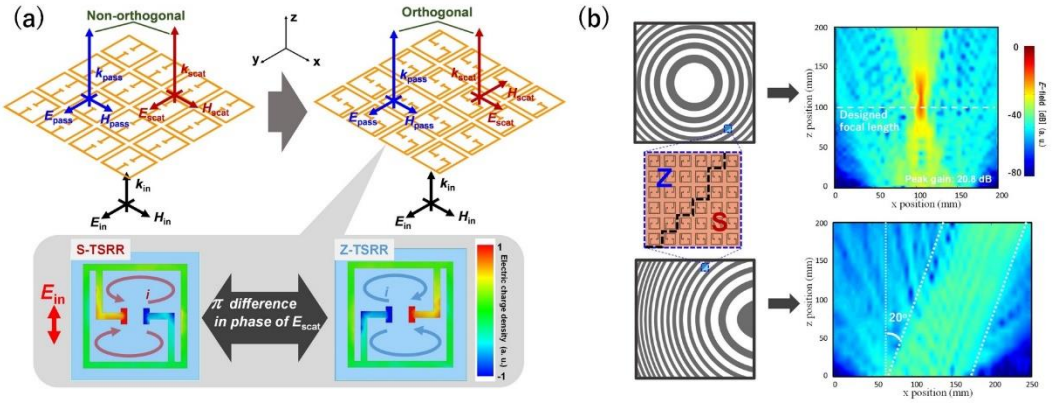

Fig. I-3. (a) Geometry of the twisted metasurface and simulated electric charges excited by incident waves. (b) Zone patterns for the twist direction and measured E-field distributions [7].

I-5. Conclusion

For 5G Evolution and 6G, in order to demonstrate and evaluate the effectiveness of the proposed solution which combines the BF function in BS with multiple passive TMSs, the mmW experimental trials have been conducted. The trials employ the 5G NSA 28 GHz-band BS that supports the analog BF and the commercial UE as the experimental equipment. When BS was installed on the rooftop of the building, only a few Mbps of DL throughput was achieved at the foot of the building, indicating that it is difficult to create the mmW coverage area at the foot. On the other hand, the trials with the proposed solution using the five TMSs showed that almost 1 Gbps maximum DL throughput was achieved in the target area. Moreover, for utilization of TMSs in much higher frequency band such as sub-terahertz band toward 6G, we show cost-effective metasurface structure and its effectiveness from a fabrication point of view.

REFERENCE

[1] NTT DOCOMO, INC., “White paper: 5G Evolution and 6G (version 5.0),” Jan. 2023. [Online]. Available: https://www.nttdocomo.co.jp/english/binary/pdf/corporate/technology/whitepaper_6g/DOCOMO_6G_White_PaperEN_v5.0.pdf

[2] M. D. Renzo, M. Debbah, D.-T. Phan-Huy, A. Zappone, M.- S. Alouini, C. Yuen, V. Sciancalepore, G. C. Alexandropoulos, J. Hoydis, H. Gacanin, J. d. Rosny, A. Bounceur, G. Lerosey, and M. Fink, “Smart radio environments empowered by reconfigurable AI meta-surfaces: an idea whose time has come,” EURASIP J. Wireless Commun. and Netw., vol. 2019, no. 1, pp. 1-20, Dec. 2019.

[3] Q. Wu and R. Zhang, “Towards smart and reconfigurable environment: Intelligent reflecting surface aided wireless network,” IEEE Commun. Mag., vol. 58, no. 1, pp. 106-112, Jan. 2020.

[4] K. Goto, S. Suyama, T. Yamada, K. Arai, O. Kagaya, “Experimental Trials with Combination of Multiple Transmissive Metasurfaces and Beamforming for mmW Coverage Enhancement,” in Proc. IEEE 98th Veh. Technol. Conf. (VTC-Fall), pp. 1-5, Oct. 2023

[5] X. Hou, X. Li, X. Wang, L. Chen, and S. Suyama, “Some observations and thoughts about reconfigurable intelligent surface application for 5G Evolution and 6G,” ZTE commun., vol. 20, no. 1, pp. 14-20, Mar. 2022.

[6] V. G. Ataloglou, M. Chen, M. Kim, and G. V. Eleftheriades, "Microwave Huygens’ Metasurfaces: Fundamentals and Applications," IEEE J. Microwaves 1(1), 374–388 (2021).

[7] D. Kitayama, A. Pander, Y. Hama, and H. Takahashi, "Alignment-free twisted-split-ring metasurface on single substrate with 2π phase range for linearly polarized sub-terahertz wave," Opt. Express 31, 20769-20786 (2023)

[8] NTT DOCOMO Press Release, “DOCOMO conducts world's first trial of transmissive metasurface on window to deliver indoor radio waves to outdoor foot of building,” Jan. 2023. [Online]. Available: https://www.docomo.ne.jp/english/info/media_center/pr/2023/0130_02.html

II. High-Performance Radio Propagation Simulation Method for Path Loss Estimation

Takahiro Tomie, Satoshi Suyama, Koshiro Kitao, Nobuaki Kuno
NTT DOCOMO, INC.

***Abstract*—To establish a simulation technology for estimating and predicting radio propagation characteristics with short calculation time and high accuracy, we have proposed a novel color images method (CIM) based on processing colors images of walls of buildings which are viewed from positions of Txs and Rxs. However, the estimation performance of the proposed CIM has not been sufficiently clarified. In this work, we compare the CIM with Wireless InSite (WI) employing a conventional ray tracing method (RTM) in terms of estimation accuracy and calculation time. Comparison results show that the average value and root mean squared error of path loss estimation errors of the CIM are much smaller than those of the WI. Moreover, the calculation time of the CIM is much shorter than that of the WI.**

II-1. Introduction

In the 5G Evolution and 6G system, massive devices are connected to many base stations (BSs) directly and/or indirectly through active or passive relay stations (RSs) such as repeaters, RISs, etc. The massive radio links of BSs and devices, BSs and RSs, RSs and devices, use various frequencies and require extreme high data rate, extreme low latency, etc. depending on use cases [1], [2]. For maximizing the performance, quality assurance, efficient system operation of the 5G Evolution and 6G systems, a technique for estimating radio wave propagation characteristics such as path loss, delay time with short computation time and high accuracy is necessary. This method also needs to be suitable for site-specific environments of the systems using the RSs. Although there are several conventional estimation methods for site-specific environments such as ray tracing method (RTM), methods based on deep learning, etc. [3]-[6], these methods still do not satisfy the requirements of short calculation time and high accuracy. Therefore, we proposed a new method named color images method (CIM) and evaluated its performance in an outdoor urban environment at 1 GHz band [7], [8]. However, the estimation performance of the proposed CIM has not been sufficiently clarified.

In this work, in order to clarify the estimation performance of the CIM, we estimate the path losses using the CIM and the RTM, and compare quantitatively the estimation accuracy and calculation time of these methods [9].

Fig. II-1. Position of the Tx and the measurement courses.

II-2. Evaluation Methods

II-2.1. Measured Data

Here, the measured path loss data set in [10], was used. Fig. II-1 shows the position of

the Tx and the measurement courses. There are 40 measurement courses in total and the courses C1-C7 are relatively long. The Tx was set on the roof top of a building with 12.5 m height from the ground. The Rx was set on the roof top of a measurement car with 1.5 m height from the ground. The Tx's antenna and Rx's antenna were dipole antennas. The Rx was moved on the measurement courses to measure path loss at frequency of 1298 MHz. After the measurement, median path loss values in 10 m length were obtained and given a total of 839 points.

II-2.2. CIM

In this section, we describe a brief overview of the CIM proposed in [7] and its calculation conditions. The CIM is based on processing colors images of walls of buildings which are seen from the positions of Txs and Rxs. For detecting and calculating the scattering waves of walls, each wall of each building in an evaluation area is assigned to a different RGB color. Then, two types of color images of the walls which are seen from the Txs and Rxs respectively, are created as shown in Fig. II-2. Next, the scattering walls are detected by the colors corresponding with these walls existed in both the Tx's image and Rx's image. By counting the number of pixels of these colors and multiplying with coefficients, the total received power P_{R} at each position of the Rx can be expressed as below:

$$P_{\mathrm{R}} = \sum_i k \cdot C(i) \cdot N_{\mathrm{P,T}}(i) \cdot N_{\mathrm{P,R}}(i) \tag{1}$$

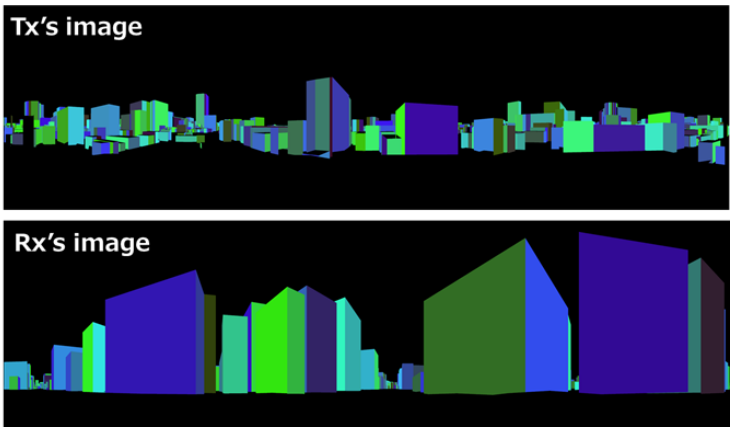

Fig. II-2. The color images viewed from the Tx and the Rx.

Where $N_{P,T}(i)$, $N_{P,R}(i)$ are numbers of pixels of the colors corresponding with the scattering wall $\#i$ in Tx's image and Rx's image, respectively. The $\#i$ can be representative for the index of the path $\#i$. The coefficient k is depending on material of the wall, the frequency and size of image. $C(i)$ is a coefficient related to the transmit power and the gains of the Tx antenna and Rx antenna.

To estimate the path loss using the CIM, the locations and conditions of the Tx and Rx were set as those described in the section II. A. The number of reception points were 839. Here, only one-time scattering was considered. The image size was 7200*3600 pixels. The coefficient k was $10^{-19.8}$. In calculation, a PC with two CPUs included 56 cores at 2.7 GHz was used. The memory size is 1 TB. The PC also has 4 GPU devices with 1280 cores per device. However, due to the current implementation of the CIM, optimal use of the CPU and GPU is not possible, so in the evaluation, only one core of the CPU and without the GPU device were used.

II-2.3. RTM

For evaluating path loss using a RTM, we use WI employing a hybrid method of an imaging method and a ray launching method [6]. Here, the positions and conditions of the Tx and Rx were set as those described in the section II. A. The ray spacing was set to 0.1 degree. The maximum number of reflections were set to 1, 2, 6, and 12, and the maximum number of diffractions were set to 1 and 2, respectively. Here, the maximum number of reflections m and maximum number of diffractions n is denoted as mRnD. The building material was assumed to be concrete. Moreover, the same PC also was used for both methods. Unlike the CIM, the WI is designed to take advantages of using the CPU and GPU devices, and minimum calculation condition is using with one core of the CPU and one GPU device. Therefore, the minimum calculation condition was used to evaluate. It means that it is not fair comparison in calculation times of two methods, but these information are needed for references.

II-3. Comparison Results

Fig. II-3 shows the comparison of the percentage of estimable reception points *Ac* of the CIM and the WI. It is found that the percentage of estimable reception points of the CIM is about 3% larger than that of the WI's 12R1D case, and in this case the difference of two methods is the smallest. Therefore, we use the WI's 12R1D case for comparisons of estimation accuracy and calculation time. It is also found that the percentage *Ac* of the CIM is about 19% or more smaller than that of the cases with maximum two-time diffractions of the WI. However, by increasing the number of scattering times of the CIM, the higher percentage *Ac* can be achieved.

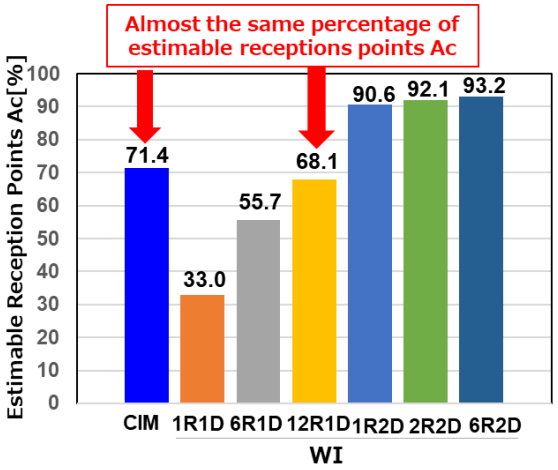

Fig. II-3. Comparison of percentage of estimable reception points of the CIM and the WI.

Fig. II-4 shows the comparison of the estimation accuracies. It is found that the average values μ and RMSE of the differences between the estimated results and the measured results of the CIM are small at -0.8 dB and 8.3 dB, respectively, while those of the WI are very large with 15.9 dB and 21.7 dB for the case of 12R1D and 12.7 dB and 15.1 dB for the case of 6R2D, respectively. This means that the estimation accuracy of the CIM is much higher than those the WI.

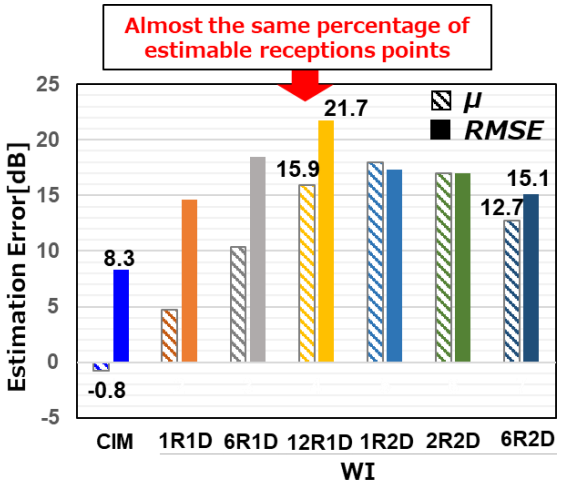

Fig. II-5. Comparisons of estimation accuracies of the CIM and WI

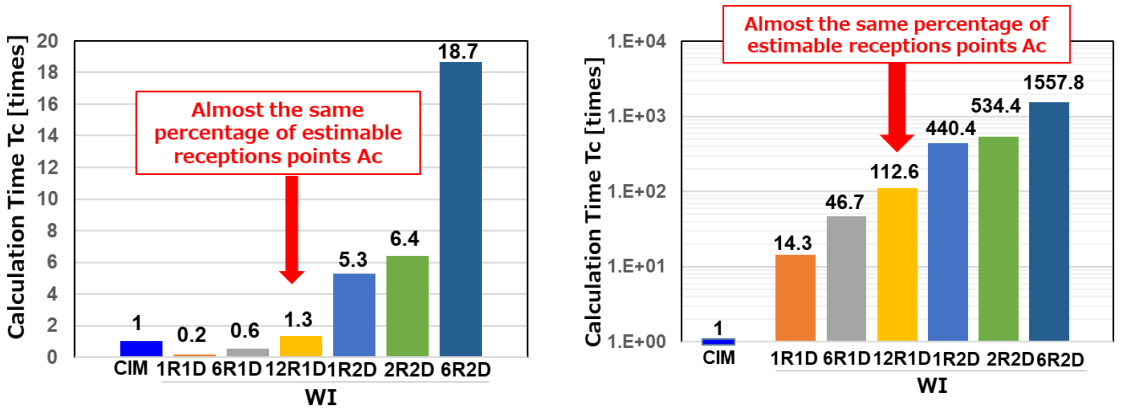

(a) Case of calculation from begin (b) Case of changing the condition of the Tx

Fig. II-4. Comparison of calculation times of the CIM and WI.

Fig. II-5 shows the reference result of comparison of calculation times. Here, the calculation times are normalized to that of the CIM. As mentioned above, this is not an appropriate comparison, since both methods used one core of the same CPU to compute, but in the case of the WI, an additional GPU device is used in advantage. Therefore, the calculation times are shown here for reference. Fig. II-5 (a) shows that, for almost the same percentage of estimable reception points, the calculation time of the CIM is 0.77 (=1/1.3) times shorter than that of the WI's 12R1D case. It means that if the WI does not use the additional GPU device, the calculation time of the CIM is much shorter than 1/1.3 time comparing with the WI. Fig. II-5 (b) shows the comparison of calculation times when the conditions of the Tx are changed, such as its position or height. In these cases, the calculation times of the CIM are 30 seconds. Here, we also normalized the calculation

times to 30 seconds. It is found that the calculation time of the CIM is 0.0089 (=1/112.6) times shorter than that of the WI's 12R1D case. The reason for this is, in the CIM, the processing of creating color images for all reception points and analyzing color of these images (pre-processing), need not do again, while in the RTM, almost processes have to redo from beginning.

II-4. Conclusion

In this work, we quantitatively compared the percentage of estimable reception points, the estimation accuracy, and the calculation time of the proposed CIM with the WI employing the conventional RTM. The comparison results shown that, for the percentage of estimable reception points, the CIM can estimate a slightly larger than the WI with maximum twelve-time reflections and one-time diffraction. We also shown that the CIM has very high estimation accuracy. Moreover, it was verified that the calculation time of the CIM is much shorter than the WI, especially in case of changing conditions of the Tx.

In future works, we plan to evaluate the estimation accuracy in various environments and frequencies, and consider using GPU devices for real-time estimation of radio propagation characteristics.

REFERENCE

[1] NTT DOCOMO, INC. “White paper, 5G Evolution and 6G (Version 4. 0),” Jan. 2022. https://www.docomo.ne.jp/english/binary/pdf/corporate/technology/whitepaper_6g/DOCOMO_6G_White_PaperEN_v4.0.pdf

[2] H. Tataria, et. al., “6G Wireless systems: Vision, requirements, challenges, insights, and opportunities,” *Proceedings of the IEEE*, vol. 109, no. 7, pp. 1166-1199, July 2021.

[3] N. Kuno, et. al., "Deep Learning-Based Path Loss Prediction Using Side-View Images in an UMa Environment," *EuCAP2022*, Mar.-Apr. 2022.

[4] S. C. Kim, et. al., "Radio propagation measurements and prediction using three-dimensional ray tracing in urban environments at 908 MHz and 1.9 GHz," *IEEE Trans. Veh. Technol.*, vol. 48, no. 3, pp. 931–946, May 1999.

[5] T. Imai, et. al., “A Propagation Prediction System for Urban Area Macrocells using Ray-tracing Methods” *NTT DoCoMo Technical Journal* Vol. 6 No.1, p. 41-51.

[6] Wireless InSite Reference Manual, Version 3.3.4.1, https://www.remcom.com

[7] T. Tomie, et. al., " A Novel Estimation Method of Radio Propagation Characteristics Based on Color Images,” *VTC2022-Fall*, 2022, pp. 1-5.

[8] T. Tomie, et. al., " A method of path loss prediction based on computer graphics technologies,” *IEICE Communications Express*, 2023 Vol. 12, No. 6, p. 300-304.

[9] T. Tomie, et. al., " Evaluation of High-Performance Radio Propagation Simulation Method in Path Loss Estimation," *VTC2023-Spring*, 2023, pp. 1-5.

[10]T. Imai, H. Iwai, S. Ichitsubo, "Radio Propagation Modeling Competition," *IEICE Technical Report*, vol. 119, no. 28, AP2019-2, pp. 7-12, May 2019.

III. Relay-Related Technologies in New Radio Network Topology (NRNT)

Daisuke Murayama, Riku Ohmiya, Tomoki Murakami,
NTT Corporation
Kenta Goto, Satoshi Suyama,
NTT DOCOMO, INC.

Abstract— **The New radio network topology (NRNT) in beyond fifth-generation (B5G) mobile network is a crucial concept for the efficient utilization of high-frequency bands, including millimeter and terahertz waves. To realize NRNT, additional technical studies and experimental evaluations are essential, particularly concerning the integration of relay nodes, including reconfigurable intelligent surface (RIS). This paper presents two experimental results conducted in indoor environments. The first experiment examines the reception power improvement achieved by developing RIS. The second experimental assess the environmental resistance resulting from the application of network topology control, which includes the integration of relay nodes.**

III-1. Introduction

As a technological concept transitioning from Beyond 5G to 6G, the NRNT has been proposed. This concept aims to enhance radio access performance and reduce power consumption by increasing links between Transmission Reception Points (TRP), such as base station (BS) antennas, mobile terminals (MT), and relay nodes, including RIS [1-4]. Additionally, traditional wireless network topologies designed on a single-cell basis are evolving into a novel configuration where large and small cells are superimposed. The NRNT brings several advantages, including expanded coverage and line-of-sight (LOS) areas, improved resistance to shielding, capacity expansion through increased multiple input multiple output (MIMO) space multiplexing, and more.

In real-world environments, the topology dynamically changes based on factors such as the environment, situation, and service demand. Therefore, control systems must exhibit adaptability to temporal fluctuations. This paper introduces relay-related technologies currently under research and development. Furthermore, we present experimental demonstrations showcasing the reception power improvement achieved by implementing RIS and the resistance to environmental changes achieved through network topology control in indoor environments, contributing to the realization of the NRNT concept.

III-2. Experimental Evaluation of Received Power Improvement Effect Using RIS

This section introduces angular profile experiments using a 28 GHz band channel sounder and presents their results to elucidate the improvement effect on reception power when RIS are installed in indoor environments. Fig. III-1 depicts the layout of the experimental environment at the NTT DOCOMO R&D Center and includes a photograph for reference. In this setup, the positions of the transmitter and RIS were fixed, while the receiver was installed in LOS and non-LOS (NLOS) conditions. The distance from the RIS to the receiver was set at 5 m and 20 m, respectively. We conducted measurements of angular profiles at each receiver position with the RIS configured to reflect signals in the receiver's direction. The measurement specifications are detailed in Table. III-1.

Fig. III-1 illustrates the measured angular profile in the environment. In the LOS condition, RIS control substantially enhanced the reception power at the receiver by approximately 20 dB. Similarly, in the NLOS environment, RIS control led to an improvement of around 11 dB in the reception power at the receiving station. Consequently, even in a multipath indoor propagation environment, significant enhancement in reception power can be achieved by dynamically adjusting the RIS based on the receiver's position. Furthermore, since RIS control has the potential to contribute to the expansion of area coverage, promising practical applications can be anticipated in the future.

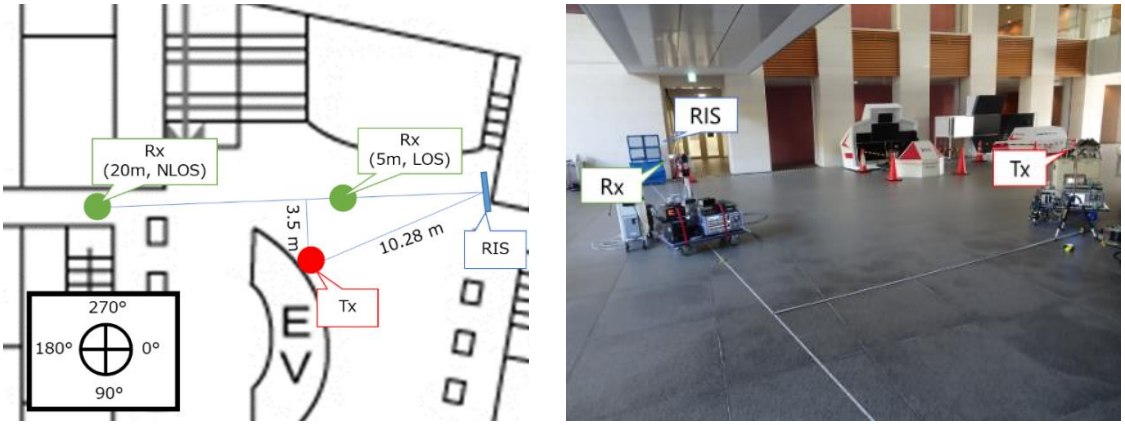

Fig. III-1. Experimental environment.

Table. III-1. Experimental specifications.

Center frequency	27.6 GHz
Bandwidth	200 MHz
Transmit power	37 dBm (5 W)
Transmit antenna (gain)	Omni (3.5 dBi)
Receive antenna (beam width, gain)	Horn (10 deg., 24.6 dBi)
Height of transmitter	1 m
Height of receiver	1 m
Height of RIS	1 m

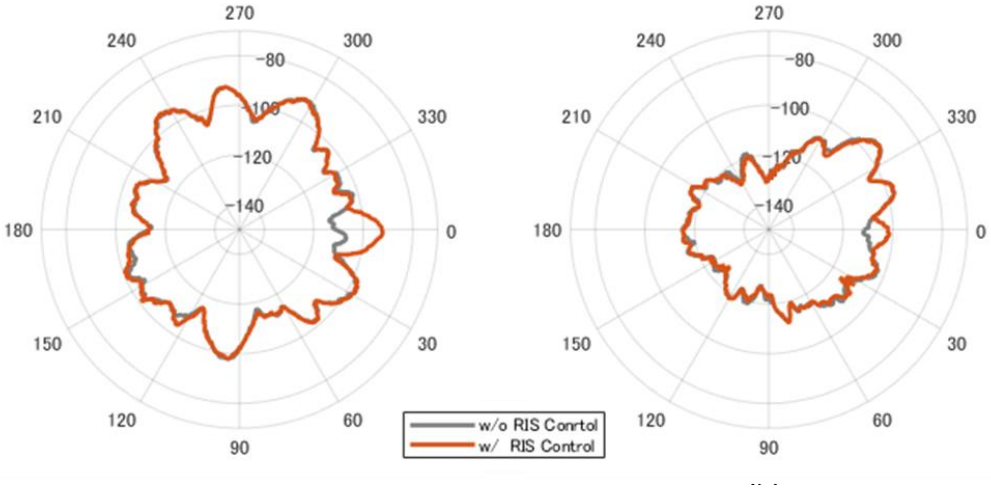

(a) 5 m position (LOS) (b) 20 m position (NLOS)

Fig. III-2. Angle profiles.

III-3. Experimental Evaluation of Fast Design and Control Techniques for Wireless Network Including Relay Nodes

NRNT networks that use multiple relay nodes have many candidates for available relay node locations and directions. A huge amount of calculation is required to automatically derive an area design that combines multiple relay nodes. For this reason, it was difficult to realize control that updates the network topology as the environment changes. Therefore, we devised a method to derive the sub-optimal placement independently for each cluster using a clustering method based on unsupervised machine learning. This method avoids the explosion in the number of placement combinations to be evaluated and enables fast derivation of network design. The procedure is shown below.

(1) Search for base station placement(s) that maximize the number of evaluation points that satisfy the required quality at the base station only, without considering the placements of relay nodes.

(2) Using the base station placement derived in (1), eliminate from the candidates relay node(s) placement(s) that do not result in reception quality higher than the threshold value.

(3) Cluster the evaluation points for which the required quality was not satisfied by the base station placement derived in (1) with the same number of relay nodes to be used, using the kmeans++ method.

(4) Search for the relay node placements that maximize the number of evaluation points that satisfy the required quality independently for each cluster calculated in (3).

(5) If the ratio of evaluation points satisfying the overall required quality is above the

threshold value, the process is terminated, and if it is below the threshold value, the process is re-derived by increasing the number of relay nodes by one.

An area quality evaluation was conducted in a shielded room at NTT Yokosuka R&D Center by creating an environment with a lot of shielding that was simulated as an indoor logistics warehouse through experiments. We assumed an environmental change from two rows of 1.24 m × 6.75 m × 2.5 m shields to four rows in an 11.8 m × 21.8 m × 2.6 m shielded room. This area was covered by a local 5G base station in the 28 GHz band connected to a WiGig AP in the 60 GHz band as a regenerative relay station. Fig. III-3 shows the network configuration and Fig. III-4 shows the measurement scenery.

Fig. III-5 (a)-(d) show color maps of the measured throughput at each evaluation point. Before the environmental change, the configuration without any repeaters in (a) could not cover the entire area with high quality, but the quality of the entire area could be improved by using a relay station as shown in (b). After the environmental change, the quality of some areas decreased without the control (redesign) in (c), but with the control (redesign) in (d) using this algorithm, the quality of all areas was maintained. The computation time was reduced to about 1/5.5 × 10^-8 under the present experimental conditions (896 candidate base station locations and 1776 candidate relay station locations), compared to the method that compares and evaluates all combinations. The above shows that the proposed algorithm can maintain high area quality while updating the area design to follow changes in the environment.

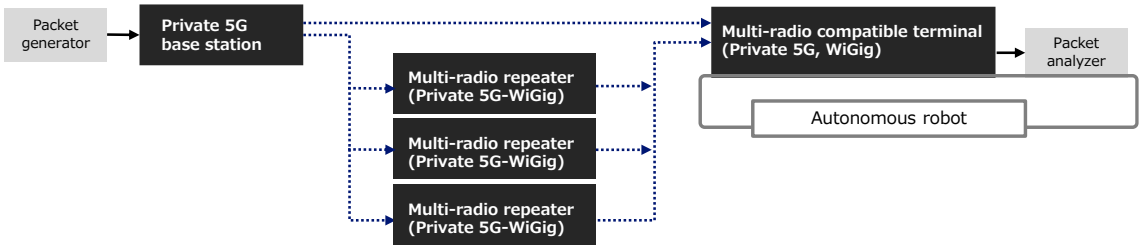

Fig. III-3. Network Configuration

Fig. III-4. Measurement scenery

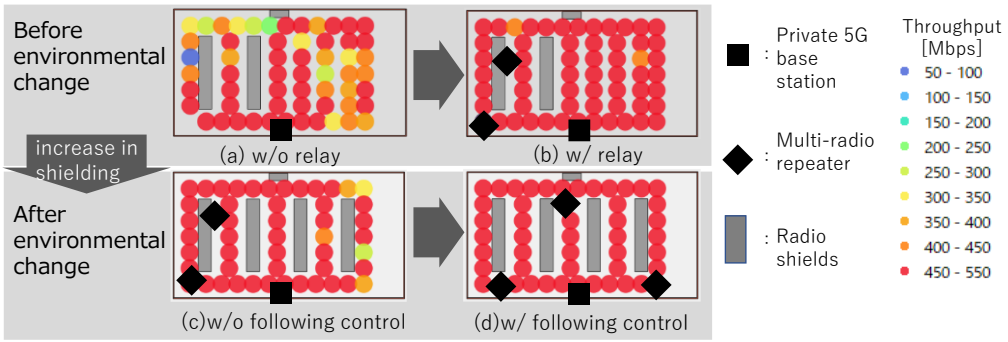

Fig. III-5. Experimental results (throughput maps)

III-4. Conclusion

We presented experiments aimed at assessing the impact of RIS on enhancing received power and evaluating tolerance to environmental changes through network topology control, crucial aspects for the realization of NRNT. In the RIS evaluation experiment, we demonstrated the dynamic alteration of the indoor propagation environment through effective RIS control. Additionally, in the network topology control experiments, we illustrated that a highly flexible network topology can facilitate rapid design derivation and control. Integrating these technologies, we aim to actualize NRNT-based networks during the 5G Evolution era.

REFERENCE

[1] NTT DOCOMO INC., “White Paper 5G Evolution and 6G (Version 5.0),” 2023. https://www.docomo.ne.jp/english/corporate/technology/whitepaper_6g/.

[2] S. Suyama, M. Iwabuchi and T. Yamada, “New Radio Network Topology for 5G Evolution and 6G,” Journal of IEICE, vol.106, No.9, pp.808-815, Sep. 2023.

[3] NTT Corporation, NTT DOCOMO INC., “NTT and NTT DOCOMO Trial First Use of User-tracking Metasurface Reflector for Extreme Mobile Coverage in Current 5G and Coming 6G Era Will enable high-speed millimeter-wave communications indoors,” https://group.ntt/en/newsrelease/2021/11/12/211112b.html

[4] I. Masashi, et al. "Intelligent radio-wave design: Distributed intelligent reflecting surface with direction-based control for millimeter-wave communications," IEICE Proceedings Series 63, IA2-2, 2020.

IV. Development of Meta-surface Reflectors for Millimeter-wave Mobile Communication Systems

Takuya Ohto, Hiromi Matsuno, Takahiro Hayashi,
KDDI Research, Inc.

Abstract—A meta-surface reflector, which directs reflected signals to an intended direction, has the potential to provide a low-cost and low-power option for signal coverage enhancement. This paper describes the development and characterization of meta-surface reflectors based on an optically transparent dual-band meta-surface reflector and a liquid-crystal reconfigurable intelligent surface. Moreover, an evaluation method for the scattering characteristics of the reflectors is provided.

IV-1. Introduction

In the fifth-generation mobile communication system (5G), 28 GHz in the millimetre wave band is assigned. In addition, a bandwidth of 15.75 GHz from the frequency band between 24.5 GHz and 86 GHz was identified as the international mobile telecommunication (IMT) band in the International Telecommunication Union (ITU) World Radiome Conference (WRC)-19 [1]. Thus, the use of the millimeter wave band is expected to increase. However, because this band suffers from high blockage loss, the received signal power in non-line-of-sight (NLOS) environments is significantly decreased. To overcome this problem, a meta-surface reflector, which has an artificial surface for reflecting signals in the nonspecular direction [2], is expected to provide low-cost and low-power consumption coverage enhancement. This reflector comprises many passive elements, and it can reflect the incident wave towards the intended direction by adjusting the reflection phase of each element and establishing a reflection link between a transmitter and a receiver in NLOS environments.

In this paper, the implementation and measurements of an optically transparent dual-band meta-surface reflector and a liquid-crystal (LC) reconfigurable intelligent surface (RIS) are presented. In addition, to estimate the coverage enhancement by deploying the reflectors, methods for evaluating the scattering characteristics are reported.

IV-2. Optically Transparent Dual-Band Meta-surface Reflector

This section describes the dual-band meta-surface reflector [3]. Fig. IV-1 (a) and (b) show a photograph of the reflector and a schematic of its unit cell, respectively. The reflector is designed for each 28 GHz band and the 39 GHz band. The former band has already been assigned, and the latter band is expected to be assigned to Japan. The unit cell comprises one cross element for the 28 GHz band and four patch elements for the 39 GHz band. The reflector also comprises three layers. Each cross element and patch

element is designed on the top and middle layers of the reflector, respectively, with a common ground plane designed on the bottom layer. Each layer comprises an optically transparent conductor sheet and is spaced with an optically transparent resin. For reflector design, a supercell structure with a periodically designed reflection phase. Because the ratio of the wavelengths of 28 and 39 GHz is approximately 4:3, the reflection phases of 28 GHz and 39 GHz are designed every 90 (=360/4)° and 120 (360/3)°, respectively. For this development, the reflector is designed to reflect the signal from 0° to 45°.

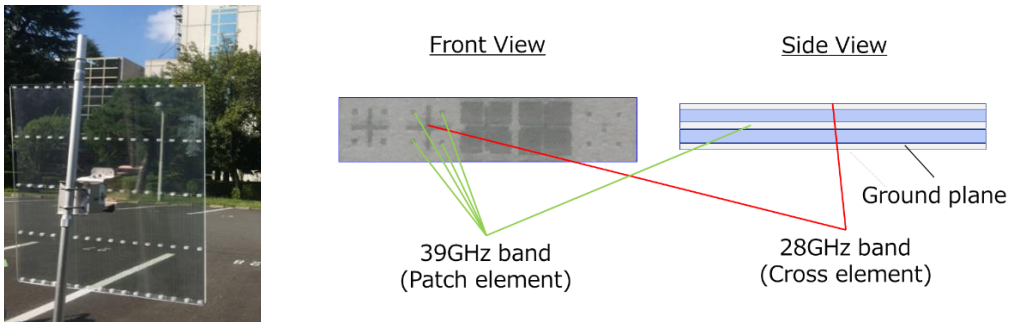

(a) Photograph. (b) Schematic of the unit cell.

Fig. IV-1. Optically Transparent Dual-Band Meta-surface Reflector.

Field testing was conducted with the developed reflector. Fig. IV-2 shows the reference signal received power (RSRP) at 28 GHz and 39 GHz. In the measurement, a reflector with a size of 790 mm×810 mm is used. As the figure shows, the RSRP of approximately 10 dB is improved by the reflector in the intended direction.

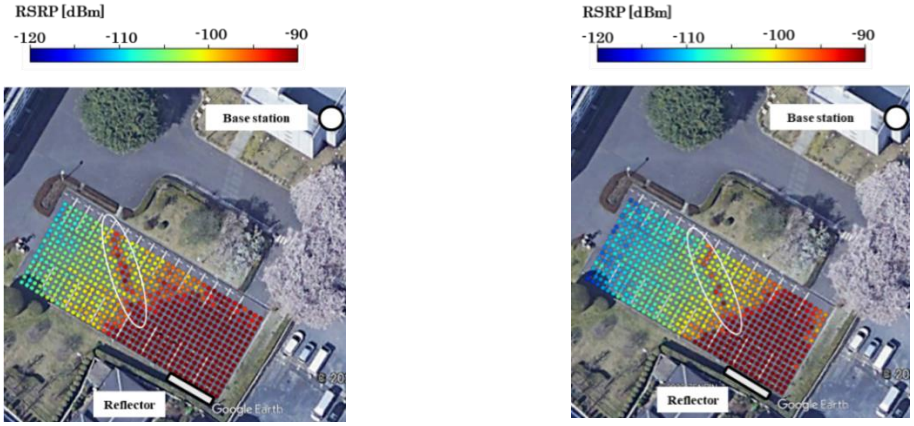

(a) 28 GHz (b) 39 GHz

Fig. IV-2. The results of field test.

IV-3. LC RIS

In this section, the LC RIS is introduced. Although the reflection angle of the meta-surface reflector in the former section is fixed once the reflector is developed, it is desirable to change the reflection angle based on the user's traffic and requirements. To address this issue, the LC RIS was developed in [4]. Fig. IV-3 (a) and (b) show

photographs of the LC RIS designed for 28 GHz and a schematic of its unit cell. The reflector utilizes LC for a reflection control functions. An LC is a molecule with anisotropy, and its electrical features, such as dielectric permittivity, depend on the direction of the molecule. The direction of the LC molecule's anisotropy is controlled by the bias voltage applied to the LC, which enables the reflector to control the reflection phase of each unit cell. As shown in the figure, the patch element is utilized not only for reflecting elements but also for the electrode for bias voltage. The bias voltage of each reflecting element is controlled via the control board. By changing the distribution of the bias voltage, the reflection direction is controlled.

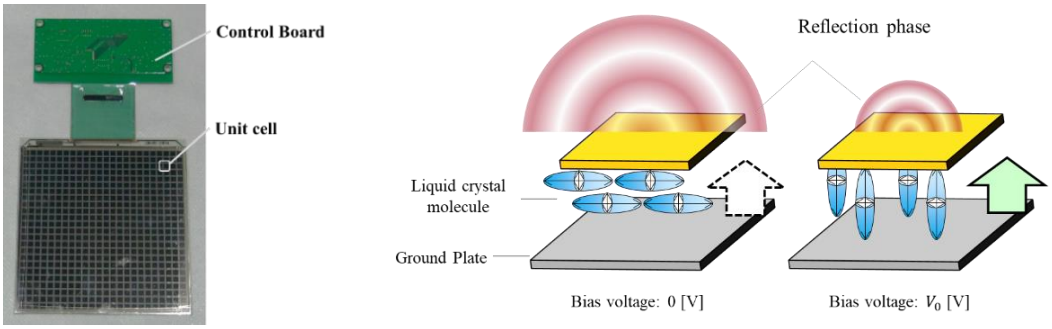

(a) Photograph. (b) Schematic of the unit cell.

Fig. IV-3. LC RIS.

Fig. IV-4 shows the scattering pattern of the LC meta-surface reflector. Each reflection direction is designed to reflect signals from 0 to 15, 30, 45, or 60 degrees, and the measurement results reveal that the reflector can reflect signals in the desired direction. Because polarized multiple-input-multiple-output (MIMO) is utilized in millimetre-wave communication systems to deliver high-speed data transmission, an IRS must also be applied for polarized MIMO. By changing the electric field length of the reflecting element, an asymmetric configuration is obtained in each polarization direction, and this reflector achieves a high cross-polarization discrimination (XPD) of more than 20 dB [4].

In addition, although an LC RIS can achieve low power consumption, there are several challenges associated with this approach, including a high reflection loss and a long response time. To address the reflection loss, the author of [5] designed the unit cell of an LC RIS to mitigate the reflection loss, and the simulation and measurement results showed that the proposed LC RIS has a maximum reflection loss reduction of more than 10 dB. Another reference [6] similarly proposed a scattering pattern design in which the reflection phase with a high reflection amplitude was selected; moreover, experimental measurements with an LC RIS showed that the reflection power can increase at the desired angle. Moreover, to address its long response time, a user and passive beam scheduling scheme based on the response time of the LC RIS was proposed in [7]. The proposed scheme selects the passive beam that provides a high data rate for multiple users. Numerical simulations show that the proposed scheme achieves a higher

throughput than does the conventional scheduling scheme, if consideration of the response time is neglected.

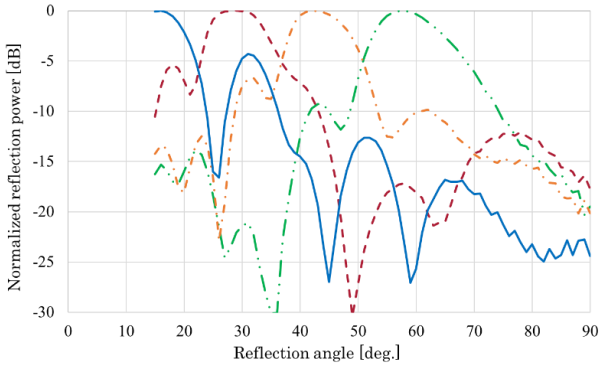

Fig. IV-4. Measurement results of scattering pattern of LC RIS.

IV-4. Evaluation Method of Meta-surface Reflector

To estimate the coverage enhancement due to the meta-surface reflector, the scattering characteristics of the reflector, such as the scattering pattern and path loss of a transmitter-reflector-receiver link, must be evaluated. In this section, an estimation method is introduced for determining such characteristics.

Table. IV-1 shows a summary of related works on the estimation methods for scattering characteristics. In reference [8], the path loss model of a transmitter-reflector-receiver link was derived based on this physical optics (PO) theorem. To utilize PO, the reflection coefficient of each unit cell should be measured correctly. However, because of the short element spacing, the reflecting element is affected by mutual coupling, and deriving or measuring the reflection coefficient, including the effects of mutual coupling, is impractical. In another approach, reference [8] reported the received power based on the radar equation (RE) using a radar cross section (RCS) of the reflector. However, because the RCS is defined in the far-field condition of the reflector and a large reflector is required to provide sufficient coverage enhancement, the use of the RE is impractical for evaluating an actual large reflector.

To address these aforementioned problems, a practical evaluation method for an actual large reflector was proposed in [9]. Upon assuming that the large reflector is composed of a combination of small reflectors (subreflectors), the RCS pattern of the large reflector is estimated by synthesizing the RCS pattern of the subreflector whose RCS pattern is measured at the usual size in the far field of the subreflector. Using numerical simulations and experimental measurements, the RCS pattern of the electrically large reflector is estimated by synthesizing the RCS pattern of the subreflectors.

Table. IV-1. Summary of works on methods for estimating scattering characteristics.

Evaluation method	Applicable conditions	Factors influencing on estimation error.
Physical optics [8]	Both of near-field and far-field of the reflector	Mutual coupling between unit cells
Radar equation [8]	Far- field of the reflector	-
Array synthesis of subreflectors [9]	Far-field of the subreflector	Mutual coupling between subreflectors

IV-5. Conclusion

This paper describes the implementation and measurement results of previously developed meta-surface reflectors. To efficiently reflect signals towards intended users, it is essential to mitigate hardware limitations associated with such reflectors. This paper also introduces works addressing the challenges of the LC RIS, namely, high reflection loss and long response time. Furthermore, because it is necessary to estimate the coverage enhancement by deploying reflectors to utilize meta-surface reflectors, existing evaluation methods for scattering characteristics were reported.

Acknowledgements

A part of this research was supported by the Ministry of Internal Affairs and Communications in Japan (JPJ000254).

REFERENCE

[1] ITU-R, “Studies on Frequency-related Matters for International Mobile Telecommunications Identification Including Possible Additional Applications to Mobile Service on Primary Basis Portion(s) of Frequency Range between 24.25 and 86 GHz for the Future Development of Internal Teleccomunication for 2020 and Beyond,” 2015.

[2] KDDI, Beyond 5G/6G White Paper ver.2.0.1, Oct. 2021.
https://www.kddiresearch.jp/tech/whitepaper_b5g_6g/

[3] C. O. Nguyen, et al., “Dual Band and Dual Polarized Reflect Array Usimg Cross Dipole and Patch Elements,” *in Proc. of ISAP2020*, pp.821-822, 2021.

[4] H. Matsuno, et al., “Development of a Dual-Polarized Direction-Variable Liquid-Crystal Meta-Surface Reflector for Intelligent Reflecting Surface,” in *IEEE Access*, , vol. 11, pp. 95757-95767, May 2023.

[5] Y. Cui, et al., "A Low-Cost Structure for Reducing Reflection Loss in Intelligent Reflecting Surface of Liquid Crystal," *in IEEE Antennas and Wireless Propagation Letters*, vol. 22, no. 12, pp. 3027-3031, Dec. 2023.

[6] T. Ohto, et al., “Reconfigurable Meta-surface Reflectors: Practical Phase adjustment method and Experimental Validation,” *in Proc VTC2022-Spring*, Helsinki, Finland, June 2022.
[7] K. Yoshikawa, et al., “User and Passive Beam Scheduling Scheme for Liquid Crystal IRS-assisted mmWave Communications” to be presented *in Proc. EuCAP2023*.
[8] W. Tang, et al., “Path Loss Modeling and Measurements for Reconfigurable Intelligent Surfaces in the Millimeter-Wave Frequency Band,” in IEEE Trans. Commun., vol. 70, no. 9, pp. 6259-6276, Sept. 2022.
[9] H. Matsuno, et al., "Practical Evaluation Method of Large Size IRS: Synthesis of Reflection Pattern of Sub-IRS," *in IEEE Access*, vol. 11, pp. 102072-102081, Sep. 2023.

V. Terminal-Collaborated MIMO Reception

Hidekazu Murata, Yamaguchi University
Satoshi Suyama and Huiling Jiang, NTT DOCOMO, INC.
Daisuke Murayama, NTT Corporation

Abstract— **In terminal-collaborated multiple-input multiple-output (MIMO) reception, the terminal to be the collaboration partner needs to be selected appropriately. In frequency-selective fading channels, it is possible to improve transmission performance by selecting the appropriate terminals for each frequency subband. Therefore, MIMO channel matrix-based schemes have been considered as subband-based terminal selection schemes. On the other hand, it is also clear that the residual error coefficient in received signal processing is a good indicator of the decoding performance. In this paper, we introduce efficient subband-based terminal selection schemes using two-stage terminal selection based on the MIMO channel matrices and the residual error coefficients, with the aim of further improving the performance of subband-based terminal selection. The error rate performance of the proposed schemes are evaluated by computer simulations. As a result, it is confirmed that the proposed schemes have superior transmission performance compared to the conventional schemes.**

V-1. Introduction

In multiple-input multiple-output (MIMO) transmission, the channel capacity depends on the smaller number of antennas on the transmitting and receiving sides. Although it is difficult to expand the number of antennas of a small terminal substantially, the number of antennas can be equivalently expanded if neighboring terminals cooperate.

In the collaborated-terminal MIMO reception technique [1], the number of receiving antennas can be equivalently expanded by jointly receiving MIMO signals from the base station (BS). For example, the transmission technology with high-speed and low-latency in high frequency bands such as the 28 GHz band is suitable for terminal collaboration links.

Terminal selection can reduce the traffic for collaboration by appropriately selecting a terminal from among multiple receiving terminals. So far, terminal selection schemes based on MIMO channel matrices and terminal selection using residual error coefficients have been proposed as terminal selection schemes.

High-speed transmission in a multipath fading environment with arriving delay waves is subject to frequency-selective fading. In this case, the channel state differs for each

subband, which is the unit into which the signal bandwidth is divided, and adaptive terminal selection for each subband is desirable.

It has been shown that collaboration terminal selection using the properties of the MIMO channel matrix can improve transmission performance as the number of subbands is increased [2]. Furthermore, it has been shown that the residual error coefficient is a good indicator to judge the decoding performance and is effective for terminal selection. However, since this method requires an attempt at decoding for terminal selection, an increase in the amount of computation can be a major issue.

If the increase in computational complexity can be accepted, it is also effective to obtain multiple decision results by changing the combination of received signals and combining the decision results. When decision is made from received signals obtained from other terminals and one's own received signal, the decision result may differ for each terminal making the decision, resulting in the concept of a terminal collaboration system including multiple detection terminals. Although this method increases the overall signal processing and processing delay, it has been shown that it can effectively improve transmission performance [3].

In this section, we first examine the overlap of terminals determined by each method using the channel matrix. Next, to improve transmission performance while reducing the computational complexity of terminal selection using residual error coefficients, two-stage terminal selection is considered: terminal selection using the channel matrix and terminal selection using residual error coefficients. The received signal processing assumes frequency-domain iterative equalization using a minimum mean-squared error filter.

V-2. System Model

The system model and frequency-domain iterative equalization are introduced in this section. Fig. V-1 shows the system model for collaboration terminal selection in terminal-collaborated MIMO reception. Assuming that each terminal is equipped with one antenna, multiple independent signals are simultaneously transmitted from the BS to the receiving terminal at the same frequency. Only the portion necessary for channel estimation received at the collaboration terminal is collected by the terminal, and the terminal is selected, and their waveforms are used for decoding.

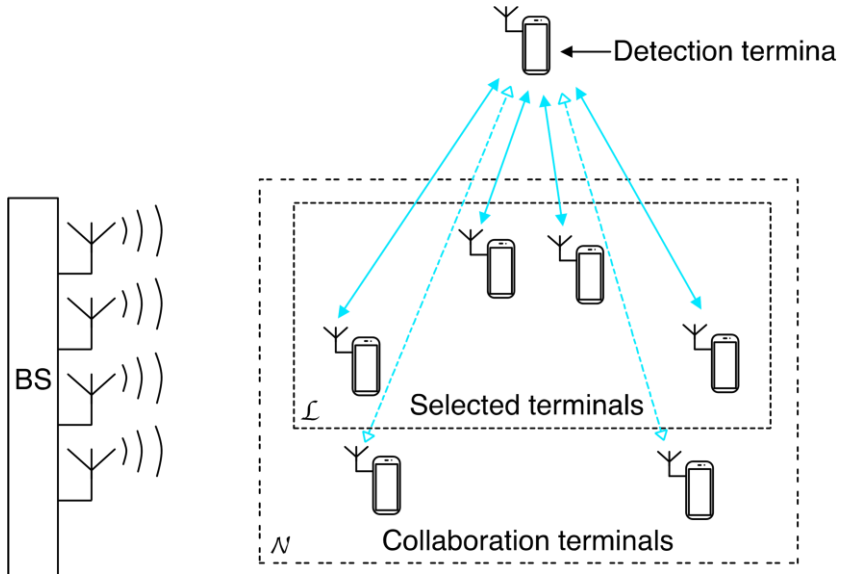

Fig. V-1. System model of terminal-collaborated MIMO reception

V-3. Subband-based Signal Processing

The transmission performance of the proposed method with respect to the number of subbands and signal-to-noise power ratio (SNR) are evaluated by computer simulation. In this study, frequency-domain soft cancellation/MMSE iterative equalization is performed as signal processing for terminal-collaborated MIMO reception. Fig. V-2 shows a block diagram of subband-based terminal selection and frequency-domain iterative equalization, where the number of BS antennas is four and the number of receiving terminals is six.

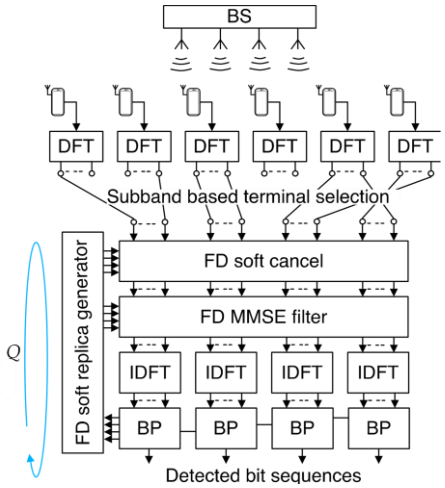

Fig. V-2. Subband-based terminal selection and iterative equalization.

As can be seen from this figure, at each terminal, the received signal is converted to the frequency domain by DFT, and the subband portion selected for each terminal is forwarded to the detection terminal. High-frequency band communication technology would be suitable for this transfer. The destination terminal performs frequency-domain iterative equalization using the signals collected from each terminal.

Fig. V-3 shows the PER performance versus the number of subband divisions S. The PER performance are shown for various selection algorithms. The one with the best performance is SIMPMC, which is a terminal selection method that uses the result of SINR estimation from the MIMO channel matrix, singular values, and the condition number to narrow down the selection candidates. Compared to the S=1 case, in which candidates are selected for all bandwidths at once, the method that selects collaboration terminals for each subband improves the PER performance by approximately one order of magnitude.

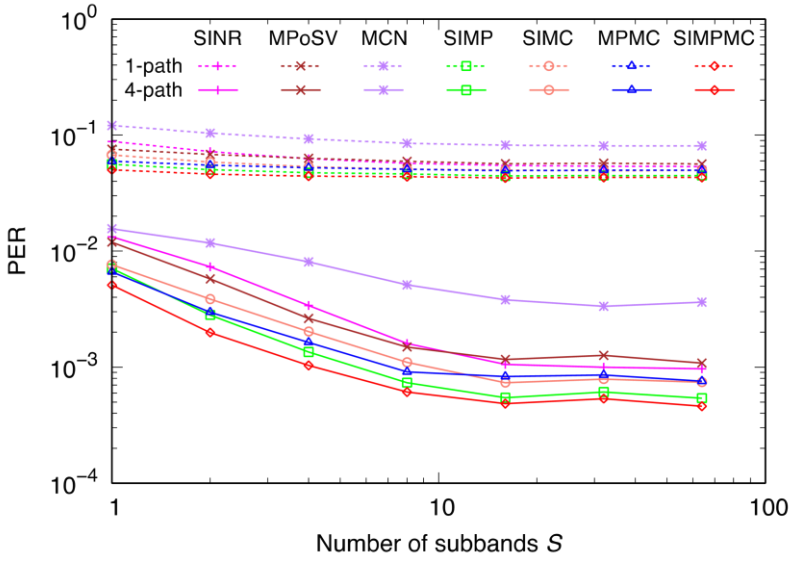

Fig. V-3. Packet error performance versus number of subbands.

V-4. Conclusion

The two-stage terminal selection for each subband using the channel matrix and the residual error coefficients in terminal-collaborated MIMO reception showed better transmission performance than the case using the channel matrix alone. The first-stage selection using the channel matrix reduced the number of terminal patterns, and the second-stage selection using the residual error coefficients improved the transmission performance while reducing the number of received signals to be decoded.

Acknowledgements

This work was supported in part by JSPS KAKENHI Grant Number JP23H00474.

REFERENCE

[1] F. Du, H. Murata, M. Kasai, T. Nakahira, K. Ishihara, M. Sasaki and T. Moriyama "Distributed detection of MIMO spatial multiplexed signals in terminal collaborated reception," IEICE Trans. Commun., vol. E104.B, no. 7, pp. 884-892, July 2020.

[2] H. Murata, "Terminal selection schemes in terminal-collaborated MIMO reception based on subband channel matrices," IEEE Communications Letters, vol. 26, no. 1, pp. 202-206, Jan. 2022.

[3] H. Taromaru, H. Murata, T. Nakahira, D. Murayama, T. Moriyama, "Error control on mobile station sides in collaborative multiple-input multiple-output systems," IEEE Access, Vol. 10, pp. 26493-26500, Mar. 2022.

VI. Beamforming-Based IRS Control for Sub-Terahertz-Band Communications in Indoor Office Environments[1]

Yasutaka Ogawa, Hokkaido University
Satoshi Suyama, NTT DOCOMO, INC.
Toshihiko Nishimura, Takeo Ohgane, Hokkaido University

***Abstract*—Using a sub-Terahertz band, we can achieve extreme high-speed communications required by Beyond 5G/6G systems. For transmission to user equipment (UE) behind an obstacle, we can employ intelligent reflecting surfaces (IRSs). According to propagation measurements in the band, we have only a few multipath components in indoor office environments. This leads to an IRS control method based on beamforming because the number of radio waves outside the optimum main beam is very small, and power that is not used for transmission from the IRS to UE is little. We apply beams generated by a Butler matrix or a DFT matrix. Simulation results show that the proposed method reveals good performance.**

VI-1. Introduction

A sub-Terahertz (THz) band is expected to play a great role in Beyond 5G/6G systems to achieve extreme high-data-rate communications. Radio waves in a sub-THz band are, however, hard to propagate behind an obstacle due to large diffraction losses. Intelligent reflecting surfaces (IRSs) can solve the propagation problem. In this paper, we investigate IRS control based on beamforming. An IRS has a set of beams. A base station (BS) sends pilot symbols, and for a different pilot, the IRS changes the beam. User equipment (UE) measures the received power for each beam, and informs the BS of the beam that provides the largest received power. The BS controls the IRS so that it can use the optimum beam providing the maximum power at the UE. This method does not need either channel state information or phase optimization. It is easy to determine the phases of the IRS. However, the performance depends on environments where it is deployed. When we have only a few multipath components in the environment, the method will work very well because the number of multipath components outside the optimum main beam is small, and power that is not used for transmission from the IRS to UE is little. According to [2], the total number of observed multipaths at 140 GHz is small in office environments. It is expected that the IRS based on beamforming works well in sub-THz bands. In this paper, we evaluate the performance using the sub-THz-band channel model proposed in [2].

[1] This paper is based on the authors' work [1].

VI-2. Beamforming-Based IRS Control

This section clarifies IRS control based on beamforming treated in this paper. Fig. VI-1 depicts the top view of a system model discussed here. Note that its multipath environment is an example. In the figure, we have two time clusters (TCs) and one subpath per TC. We express azimuth angle as ϕ. The direct path from the BS is blocked by an obstacle, and the UE is in a non-line-of-sight environment. The IRS reflects the incident radio waves toward the UE that has a single antenna. The IRS consists of $Q \times Q$ reflecting elements with half-wavelength spacing, where Q is a power of 2.

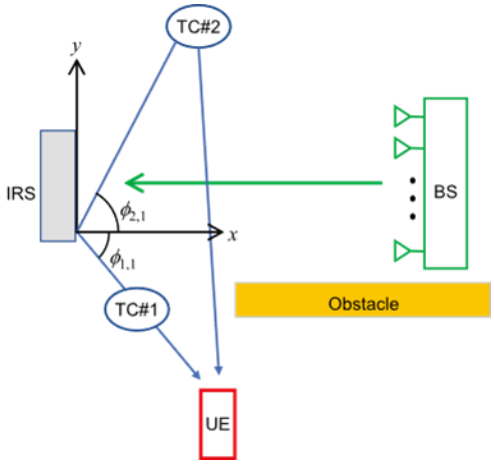

Fig. VI-1. An IRS-assisted wireless network (Top view).

We have four sets of beams, and call them codebooks in this paper. The codebooks are defined as follows:

1. Codebook BB consisting of Q^2 beams formed by phases of a Butler matrix for both the azimuth and the elevation directions
2. Codebook DB consisting of Q^2 beams formed by phases of a DFT matrix for the azimuth direction and phases of a Butler matrix for the elevation direction
3. Codebook BD consisting of Q^2 beams formed by phases of a Butler matrix for the azimuth direction and phases of a DFT matrix for the elevation direction
4. Codebook DD consisting of Q^2 beams formed by phases of a DFT matrix for both the azimuth and the elevation directions

The reason why we use the four codebooks will be clarified later. It should be noted that we do not have either Butler matrix circuits or DFT matrix circuits. Phases realized by those circuits are given to phase-shift devices.

The beam patterns in the azimuth domain are shown in Fig. VI-2 for codebooks BB and DB, where $Q = 8$ and elevation angle $-7.2°$. Since we have 64 elements, the maximum gain is 18 dB. Note that we assume that each IRS element works as an isotropic antenna with 0 dBi gain. From the figures, we see that the gain at angles where two beams cross

each other is about 14 dB. This means that if we use a single codebook, we have about 4 dB degradation in the worst case. Furthermore, it is seen that beams of one codebook have the maximum gain around angles where beams of the other codebook have the lowest value, and that beams of both codebooks help each other. The degradation is reduced to about 1 dB. This is the reason why we use both the Butler matrix and DFT matrix codebooks. We have stated the azimuth case so far, but the situation is the same also for the elevation. Thus, we have BB, DB, BD, and DD in all. The four codebooks improve the performance comparing with the single codebook BB. In the next section, it will be shown that the performance of the four codebooks is much better than that of the single codebook BB.

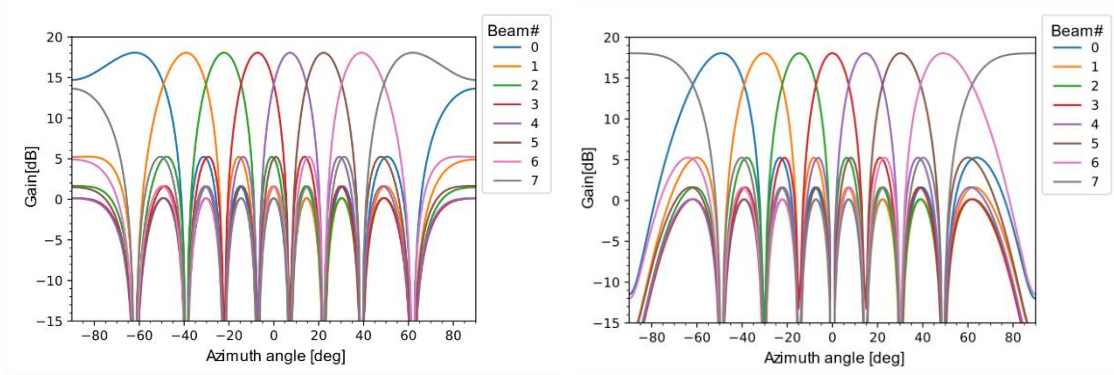

(a) Codebook BB. (a) Codebook DB.

Fig. VI-2. Beam patterns in the azimuth domain for codebooks BB and DB. $Q = 8$ and elevation angle –7.2°.

Now, we explain the IRS control in more detail. The BS sends pilot symbols. Each symbol has L equal-amplitude components at equal frequency intervals in a communication band. We choose the beam that maximizes the received power. The reason why we use multiple frequency points is because we want to choose the beam that maximizes the received power in frequency-selective fading environments due to multipath delay.

VI-3. Simulations

We evaluated the performance of the IRS based mainly on the channel model proposed in [2]. The main simulation parameters are listed in Table. VI-1. We examined two cases of multipath propagation, where the number of multipath components is 3 and 6. Refer to [1] for detail simulation parameters.

Table. VI-1. Simulation parameters.

Frequency range [GHz]	140 ~141
Number of IRS elements, $Q \times Q$	8×8
Number of frequency points in each pilot symbol, L	11
Number of trials	1000

Now, we present simulation results. We conducted 1000 trials changing the azimuth angles of departure, elevation angles of departure, and multipath phases. Fig. VI-3 and 4 show the cumulative distributions of relative received power for 3-path and 6-path cases, respectively. The legends are defined as follows:

"Butler and DFT matrices" is the distribution for the beamforming method using the four codebooks proposed in the previous section.

"Butler matrix" is that using the single codebook BB.

"Upper bound" is the distribution of received power in a case where we could optimize the IRS phases for all the L frequency points.

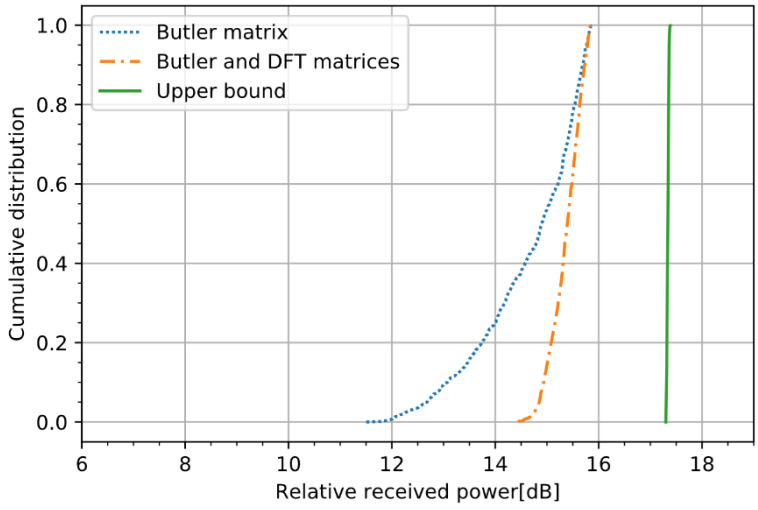

Fig. VI-3. Cumulative distributions of relative received power for 3-path case.

We see form these figures that the performance of 3-path scenario (fewer-multipath case) is better than that of 6-path one (more-multipath case). The reason for this has been stated in Section 1. For the 3-path case, the degradations of the proposed four-codebook method from the upper bound are only 1.98 dB and 2.56 dB at the cumulative distributions of 50 % and 5 %, respectively. We think that those degradations are small. Even when we have as many as 6 multipath components, the degradations are less than 4 dB. From these results, we can say that the proposed method is useful for IRS control in sub-THz bands.

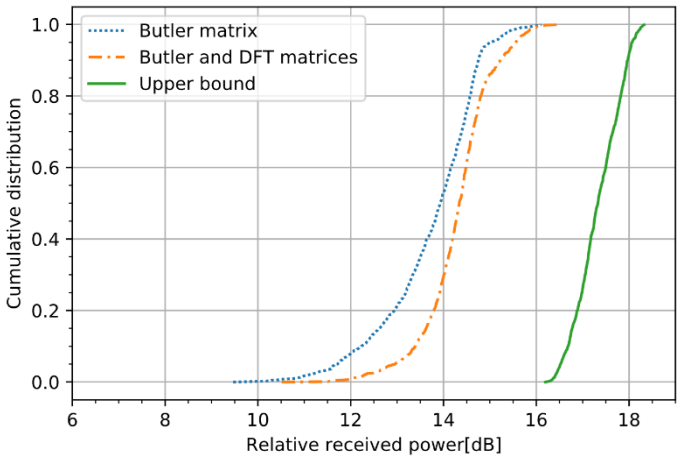

Fig. VI-4. Cumulative distributions of relative received power for 6-path case.

VI-4. Conclusion

IRSs enable to realize communications overcoming the propagation problem in sub-THz bands. Since the number of multipath components is small in the band, we have proposed the IRS control based on beamforming that is realized by phases of a Butler or DFT matrix. This method can avoid difficult channel estimation and phase optimization problems. Simulation results have shown that it reveals good performance in the sense that the received power is not so lower than the upper bound value.

REFERENCE

[1] Y. Ogawa, S. Tadokoro, S. Suyama, M. Iwabuchi, T. Nishimura, T. Sato, J. Hagiwara, and T. Ohgane, “Smart radio environments with intelligent reflecting surfaces for 6G sub-Terahertz-band communications,” IEICE Trans. Commun., vol. E106-B, no. 9, pp. 737–747, Sept. 2023.

[2] S. Ju, Y. Xing, O. Kanhere, and T. S. Rappaport, “Millimeter wave and sub-Terahertz spatial statistical channel model for an indoor office building,” IEEE J. Sel. Areas Commun., vol. 39, no. 6, pp. 1561–1575, June 2021.

VII. Beam Squint-aware Frequency Resource Allocation for IRS-aided Communication

Hiroaki Hashida, Ei Tanaka, Yuichi Kawamoto,
Tohoku University
Masashi Iwabuchi, Riku Omiya, Yoghitha Ramamoorthi, Tomoki Murakami,
NTT Corporation

Abstract—**An intelligent reflecting surface (IRS) is a device that reflects radio waves in any direction by setting the phase shift of the reflecting elements. This is expected to solve the problems of high-frequency band communications, such as vulnerability to obstacles, and realize super-multiplex connections in the high-frequency band. Considering the reflective elements of the IRS can only be time-division controlled and can support only one user per time slot, it is highly likely that a large number of resource blocks will be allocated to a single user to perform communication. However, in such a scenario, the frequency efficiency is reduced because of the effect of the beam squint. In this paper, we demonstrate the effectiveness of a method proposed to increase the frequency efficiency by optimizing the reflection direction through resource allocation and IRS phase control.**

VII-1. Introduction

To support sixth generation (6G) ultra-high-speed and high-capacity communications, attention has been focused on high-frequency bands capable of utilizing a wide frequency range. However, high-frequency bands are more susceptible to diffraction and blockage by obstacles than low-frequency bands. Intelligent reflective surfaces (IRS) offer a plausible solution to this problem [1]. IRS is a device that integrates a large number of reflective elements in a planar fashion, each of which is capable of controlling the amplitude and phase of the incident signal. By incorporating IRS into the network and intelligently controlling the reflections, problems in the high-frequency band can be effectively solved [2]–[4]. By their nature, IRS can only perform time-division control and generally support only one user per time slot. Therefore, when multiple users are supported by the IRS, the communication request of one user should be satisfied in a small number of timeslots; therefore, a large resource block (RB) is allocated to one user for communication. However, in such a scenario, the frequency efficiency is reduced because of the beam squint effect [5,6]. In this paper, we propose an IRS control and

frequency allocation scheme that effectively uses a beam squint to maximize the frequency efficiency of the IRS.

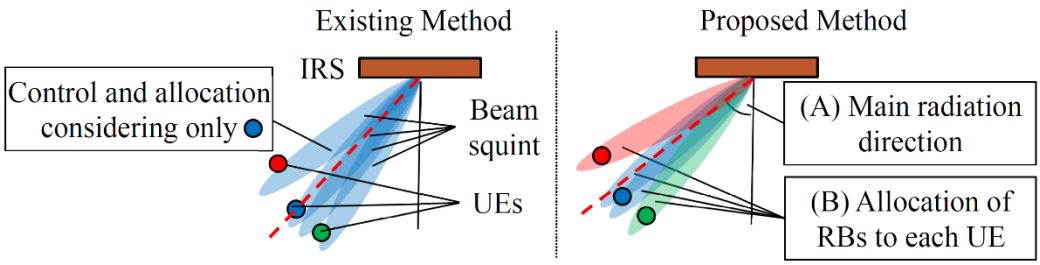

Fig. VII-1. Illustrative representation of existing method and proposed method.

VII-1.1. What is Beam Squint?

Beam squint refers to a phenomenon in which the direction of reflection of an IRS changes based on its frequency of incidence. The misalignment of the reflection direction caused by the beam squint is expressed by (1).

$$\sin\theta = \left(1 - \frac{f_c}{f}\right)\sin\theta_{\text{in}} + \frac{f_c}{f}\sin\theta_{\text{c}} \quad (1)$$

where f_c and θ_c denote the center frequency and its reflection direction, respectively, θ_{in} denotes the angle of the radio wave incident on the IRS, and f, θ denotes the frequency incident on the IRS and its reflection direction.

VII-1.2. Control Parameters of Proposed Method

We propose an IRS control and frequency allocation scheme for multiple user equipments (UEs) that makes effective use of a beam squint to maximize the frequency efficiency of the IRS. Therefore, the proposed method is effective for communicating with multiple UEs. From (1), the direction of reflection θ at a given frequency f depends on the variables θ_c and f (θ_{in} is a constant that indicates the angle of incidence from the base station (BS) to the IRS). Specifically, as shown in Fig. VII-1, the direction in which reflection control should be applied needs to be considered as well as which RBs should be assigned to UEs based on the misalignment of the reflection directions for each RB. The existing method allocates all available RBs to one UE, and the main radiation direction is perfectly directed to the UE. In other words, by optimizing the following two parameters, the beam squint can be effectively utilized and the frequency efficiency of communication through the IRS can be maximized. The two parameters are as follows: (A) the main radiation direction controlled by the phase of the IRS and (B) the allocation of RBs to UEs. (A) changed θ_c in (1). For (B), f changes based on which RB and UE is assigned determines the angle of presence θ_{UE} of the UEs and the direction of reflection θ of the assigned RB. (When $\theta_{\text{UE}} = \theta$, the IRS has the maximum gain for the UE.) The

proposed method determines (A) and (B) to maximize (capacity of all UEs)/(bandwidth) in an environment with multiple UEs. In this study, (A) is treated as a discrete value with 0.1-degree increments, and both (A) and (B) are determined by brute force to demonstrate the upper performance limit of the proposed method.

VII-2. Performance Evaluation

VII-2.1. Environment

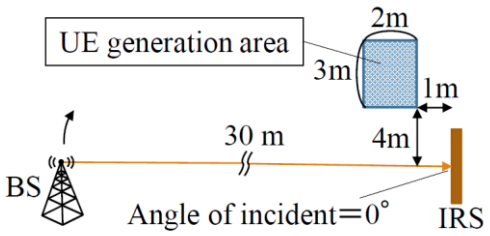

Fig. VII-2. Simulation environment.

In this evaluation, the environment shown in Fig. VII-2 was verified. n UEs were generated in the UE generation area in a uniform distribution. Ten RBs were randomly selected from 268 RBs available at 28 GHz. The available RBs were randomly selected from 10 of the 268 RBs available for communication in the 28 GHz. It was assumed that the direct waves reaching the UEs from the BS were completely blocked by obstacles, as shown in Fig. VII-2. The antenna gains of the BS and UE were set to 0 dBi because the performance of the BS and UE antennas was not relevant in this simulation. We verify the effectiveness of the proposed method by comparing it with the existing method of IRS time-division communication. Specifically, the available RBs were randomly selected from 10 of the 268 RBs assigned to the UE closest to the IRS, and the main radiation direction of the IRS was set to the direction of the UE's presence. The evaluation index indicates the frequency efficiency [bit per sec (bps)/Hz] of the communication for n UEs. In this study, the heights of BS, IRS, and UEs were assumed to be equal, and only the direct path between BS and IRS and the direct path between the IRS and UEs are considered without considering the path reflected from the ground or obstacles.

VII-2.2. Results

The results of the simulation evaluation of the environment described in the previous section are presented in Fig. VII-3 and Fig. VII-4. Fig. VII-3 shows the results when the number of UEs n is varied. Fig. VII-3 shows the results when the BS is moved upward in Fig. VII-1, and the angle of the radio wave incident on the IRS is varied from 0°. Each plot represents the average of 100 simulations. This is because randomness exists in the generation of UEs and the available RBs. First, Fig. VII-3 shows that the proposed method becomes more dominant as the number of UEs n increases. This is

because as the number of UEs increases, the probability of the existence of UEs that can gain more by beam squinting increases. Fig. VII-4 shows that when the angle of incidence of the radio wave incident from the BS to the IRS changes and the IRS controls the reflection to an angle farther from the specular reflection, the proposed method shows stable performance, whereas the performance of the comparative method deteriorates. This is because as shown in (1), the comparative method is more susceptible to the negative effects of the beam squint, because the beam shift from one RB to another increases as the angle of incidence changes.

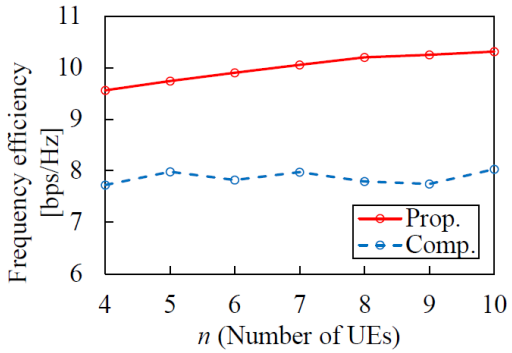

Fig. VII-4. Frequency efficiency per number of UEs

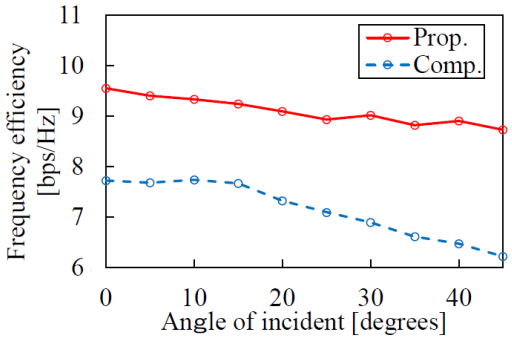

Fig. VII-3. Frequency efficiency with respect to angle of incident

VII-3. Conclusion

Beam squint negatively affects existing IRS control methods. In this paper, by optimizing the IRS reflection direction control and resource allocation, a beam squint was effectively utilized to increase the frequency efficiency of IRS-based communications. It was demonstrated that the proposed method is more effective in environments with dense UEs and high beam squint.

REFERENCE

[1] M. Agiwal, A. Roy, and N. Saxena, “Next generation 5G wireless networks: A

comprehensive survey," *IEEE Commun. Surveys Tuts*, vol. 18, no. 3, pp. 1617-1655, 3rd Quart. 2016.

[2] R. Hibi, Y. Kawamoto and N. Kato, "Standalone-Intelligent Reflecting Surface Control Method Using Hierarchical Exploration by Beamwidth Expansion and Environment-Adaptive Codebook," *IEEE Transactions on Vehicular Technology*, vol. 69, no. 5, pp. 3313-3351, May 2021.

[3] H. Hashida, Y. Kawamoto, and N. Kato, "Intelligent reflecting surface placement optimization in air-ground communication networks toward 6G," *IEEE Wireless Communications*, vol. 72, no. 9, pp. 11990-12000, Sept. 2023.

[4] Y. Liang et al., "Large Intelligent Surface/Antennas (LISA): making reflective radios smart," *Journal of Communications and Information Networks*, vol. 4, no. 2, pp. 40-50, June 2019.

[5] E. Tanaka, Y. Kawamoto, N. Kato, M. Iwabuchi, R. Ohmiya, and T. Murakami, "Exploiting Reflection Direction Variation for Phase Control in Multiple Simultaneous IRS Links," *2023 IEEE 97th Vehicular Technology Conference*, Florence, Italy, 2023.

[6] E. Tanaka, Y. Kawamoto, N. Kato, M. Iwabuchi, Y. Ramamoorthi, T. Murakami, "Frequency Resource Allocation for IRS-aided Communication using Beam Squint Approach," 2024 IEEE 21th Consumer Communications & Networking Conference (CCNC 2024), Las Vegas, NV, USA, Jan. 2024.

VIII. Prototype and Evaluation of Intelligent Reflecting Surface for 60 GHz Band

Hiroyuki Uno, Hiroyuki Uejima, Hirofumi Kosaka, Ken Katsurashima,
Panasonic System Networks R&D Lab. Co., Ltd.
Ryuhei Hibi, Yuichi Kawamoto,
Tohoku University

***Abstract*— Intelligent Reflecting Surface (IRS) is gaining recognition as a new technology component to realize B5G/6G. It enables to manipulate the phase shift of the incident wave, thereby providing control over the propagation of electromagnetic waves. This paper outlines a prototype IRS for 60 GHz band, the analyzed results by the electromagnetic simulation, and the results of characterization experiments developed by this research group.**

VIII-1. Introduction

Commercial services for the 5th generation mobile communication system (5G) have been launched in Japan since 2020, and B5G/6G, the next generation mobile communication system, is currently being considered toward the further advancement of communication services [1]. For B5G/6G, the use of millimeter wave bands and sub-terahertz bands, which are higher than microwave bands and quasi-millimeter wave bands used in 5G, is being considered to achieve further high-speed and high-capacity communications. These high-frequency bands have the feature that strong rectilinear propagation and large propagation loss have less chance of going around to the back of shielding objects such as buildings compared as microwave bands used in conventional mobile communication systems, and thus the communication range becomes significantly narrow. Therefore, this problem is a major issue to be considered for achieving the realization of the future B5G/6G.

As one of the methods to solve such problems, the utilization of intelligent reflecting surface (IRS) has garnered interest, and its research and development have been actively carried out [2]-[4]. The IRS is a reflector consisting of a planar array of microscopic structures called meta-surface. By changing the reflective properties of each unit-cell forming the meta-surface, the direction of reflection of radio waves incident on the IRS can be controlled in the desired direction. The IRS enables radio waves from base stations to reach users while avoiding shielding, thereby contributing to the expansion of areas where a good communication environment can be provided.

Various IRSs using switching devices, liquid crystals, and so on have been proposed [5],[6], however, there are few research examples corresponded to millimeter wave bands. In this paper, we introduce the design and results of the characterization experiment of

the prototype IRS using the 60 GHz band, which our research group has developed based on various studies [7]. The choice of 60 GHz band was determined by the operating frequency of the radio equipment used for wireless communication tests and is also intended to verify the applicability to millimeter waves and sub-terahertz waves that will be used in future B5G/6G.

The rest of this paper is organized as follows. The design of the prototype IRS and the results of reflection characteristics using electromagnetic (EM) simulation are introduced in Section 2. Section 3 shows the experimental results. Finally, we offer our conclusion in Section 4.

VIII-2. Design and Simulation of Prototype IRS

VIII-2.1. Configuration

Fig. VIII-1 shows the overall configuration of the prototype IRS. Our designed IRS consists of the IRS board and the electrical control board. In Fig. VIII-1, the meta-surface formed by 6,400 unit-cells is equivalent to the phase control block of the IRS board. A unit-cell is composed of reflective element and PIN diode, and the ON/OFF state of each PIN diode is controlled by the MCU block in the electrical control board. By optimizing the ON/OFF control of PIN diodes, the direction of reflection of radio waves incident on the IRS board can be controlled.

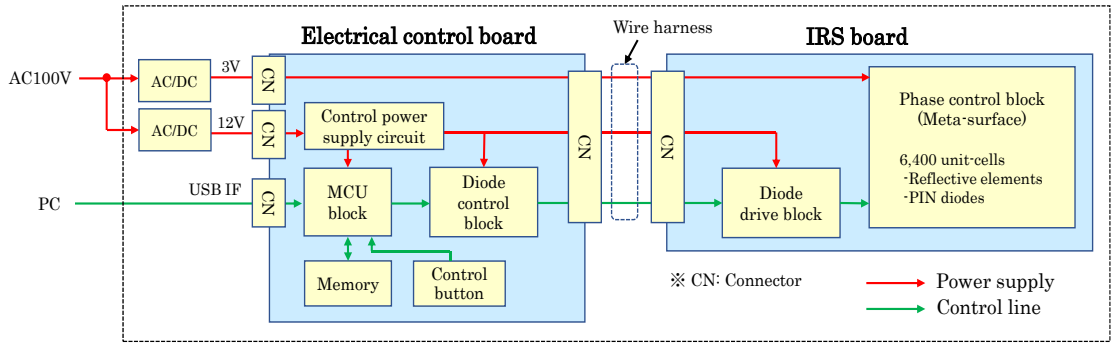

Fig. VIII-1. Overall configuration of prototype IRS.

VIII-2.2. EM Simulation Model

The EM simulation model of the IRS board is shown in Fig. VIII-2. The IRS board is composed of numerous unit-cells that arranged in reticular pattern on the +Z side plane of the dielectric substrate as shown in Fig. VIII-2 (a) and can control the reflection direction by adequately setting the reflection phase of each unit-cell. The EM simulation is perfomed with 256 elements due to work station peformance. Fig. VIII-2 (b) illustrates the unit-cell that composed of linearly polarized reflective element with side length of Lp and height of $T1$, dielectric substrate, stub via, choke stub, and PIN diode. The dielectric substrate is used R-5775 (Panasonic), and its relative permittivity (εr) and loss tangent

(tanδ) are set to 3.55 and 0.005 respectively in the simulation. The length of stub via is determined to optimize the reflection phase and the choke stub is formed to prevent the RF signal of 60 GHz from entering the control bias line. The PIN diode, which is used MA4AGFCP910 from M/A-COM, is changed ON state or OFF state by suppling a DC bias (*Vd*) and a control voltage (*Vc*), thereby be able to switch the reflection phase of the unit cell to either 0 degree or 180 degrees.

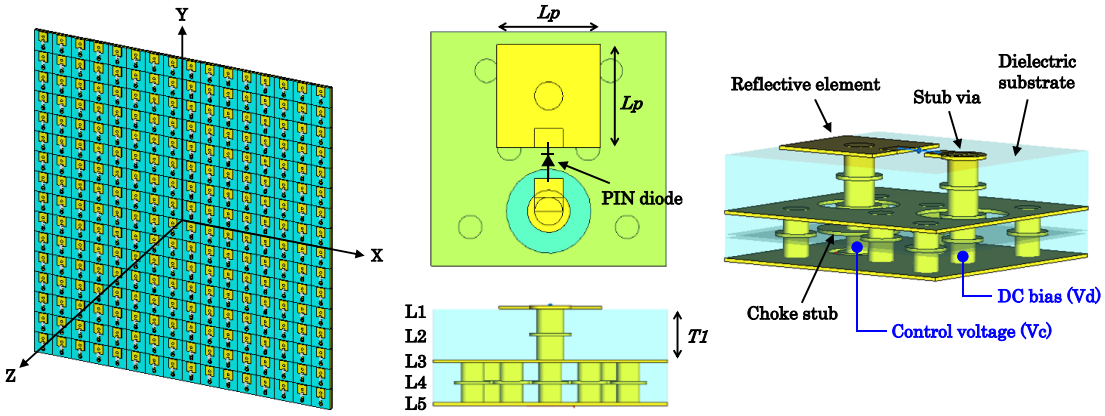

(a) (b)

Fig. VIII-2. EM simulation model of IRS board.

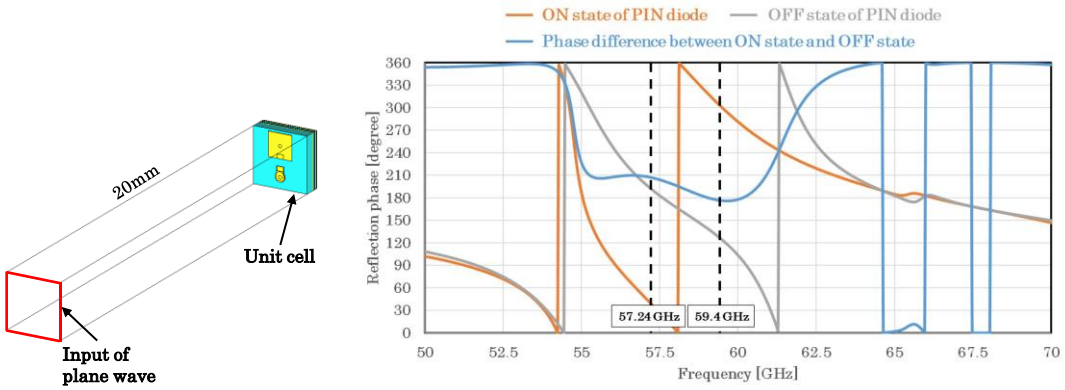

(a) (b)

Fig. VIII-3. Simulation model and results for reflection phase of unit-cell.

VIII-2.3. EM Simulation Results

VIII-2.3.1. Reflection Phase of Unit-cell

Fig. VIII-3 shows the simulation model and results for the reflection phase of unit-cell. Fig. VIII-3 (a) is the simulation model of the reflection phase, and Fig. VIII-3 (b) is

the simulated reflection phase as a function of frequency. This simulation uses CST studio suite's the finite element method (FEM), with the lateral boundaries of the unit-cell set as periodic boundary condition. The PIN diode is modeled as lumped parameter elements and its equivalent circuit for 60 GHz band is extracted from S-parameters. The ON state is modeled as a series of R = 5.2 Ω resistors and L = 0.8 nH inductors, whereas the OFF state is modeled as a series of C = 0.105 pF capacitors and R = 3 Ω resistors. Moreover, the side length *Lp* and the height *T1* of patch element is set to 1.17 mm and 0.3 mm, respectively.

As shown in Fig. VIII-3 (b), it can be seen that the phase difference between the ON state and OFF state is adjusted to approximately 180 degrees for an operating frequency (57.24 - 59.4 GHz) of wireless communication tests.

VIII-2.3.2. Reflection Characteristics of IRS Board

This chapter presents the simulation results of the reflection characteristics for the IRS board shown in Fig. VIII-2. In this simulation, the far-field pattern of radar cross section (RCS) is analyzed when the Y-axis linearly polarized plane wave is incident from the +Z direction and each PIN diode is adjusted as shown in Fig. VIII-4. In Fig. VIII-4, the red part and the blue part are the ON state and the OFF state, respectively. By using these the ON/OFF map of PIN diodes, the reflection angle θc of IRS can be adjusted to 15, 30, and 45 degrees, with the front of the incident direction set to 0 degrees.

Fig. VIII-5 shows the simulated far-field patterns of the reflected wave at 58.32 GHz. The refection angle θ at horizontal axis indicates the angle of inclination from the +Z direction to the +X direction for the XZ plane. From the simulated results shown in Fig. VIII-5, it can be confirmed that the reflected wave is tilted to the desired direction.

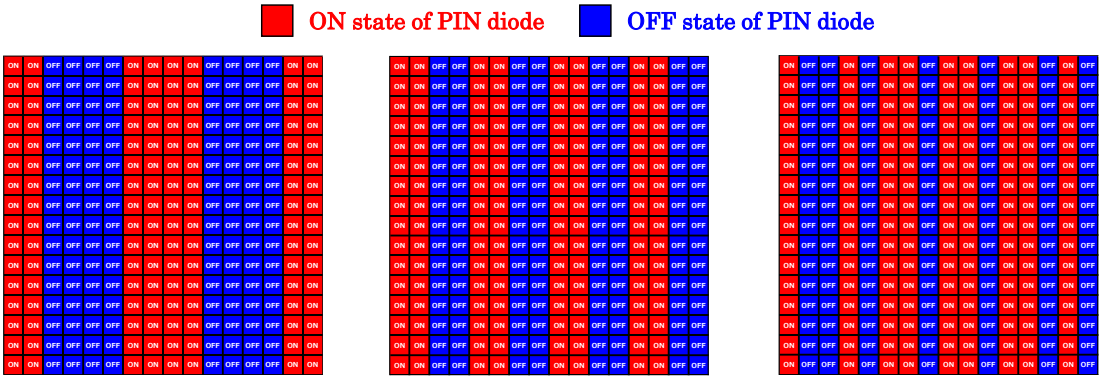

(a) θc is 15 degrees (b) θc is 30 degrees (c) θc is 45 degrees

Fig. VIII-4. ON/OFF map of PIN diodes.

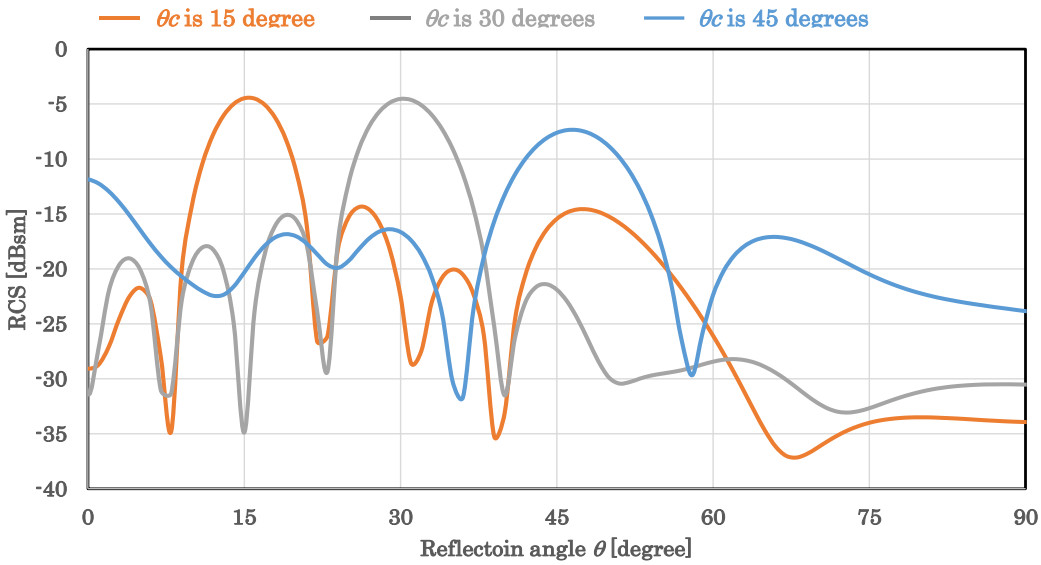

Fig. VIII-5. Simulated far-field patterns of reflected wave at 58.32 GHz.

VIII-3. Characterization Experiments

VIII-3.1. Prototype IRS Outline

Prototype IRS shown in Fig. VIII-6 consists of a total of 6,400 elements, 80 each in the Y-axis vertical and X-axis horizontal directions. Element placement area is 200 mm x 200 mm, Element spacing is 2.5 mm, and Element size is 1.5 mm x 1.5 mm. Supported frequency is 58.32 GHz, and reflection phase control is a binary control of 0/180 degrees.

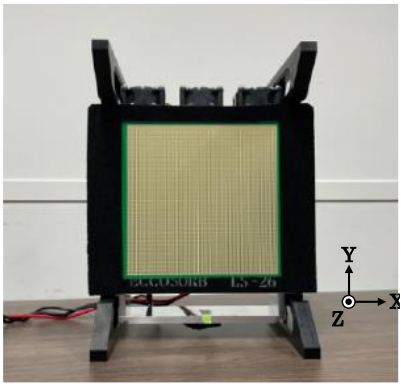

Fig. VIII-6 Prototype IRS.

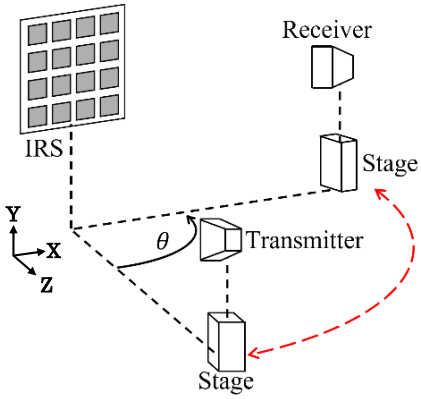

Fig. VIII-7. Experimental environment.

VIII-3.2. Experimental Environment and Methods

In this experiment, IRS, transmitter, and receiver are arranged as shown in Fig. VIII-7, and the reflection characteristics of the IRS are evaluated by changing the position of the receiver in the direction indicated by the arrow line. The transmitter is a communication device using 60 GHz band by Panasonic and the receiver is an Anritsu

MS2762A spectrum analyzer. The direction of reflection of IRS is set to four patterns of 0, 15, 30, and 45 degrees, with the front of the incident direction set to 0 degrees. The receiving angle θ between the transmitter, IRS, and receiver is changed from 10 to 60 degrees in 1-degree increments. The distance between transmitter and IRS and between receiver and IRS are both 10 m. This experiment is conducted in a large anechoic chamber.

VIII-3.3. Experimental Results

Fig. VIII-8 shows the experimental results. The angle θc shows the primary radiation direction of the reflected wave by the phase control of IRS. The results show that the received power peaks at 1 degree inside of each primary radiation direction. This is due to the characteristics of the device. The results also show that the peak in the primary direction is moderate and that the received power is not stable in the non-primary direction. This may be due to several factors. One of the major factors is that the experimental environment is small compared to the IRS, which is designed for long-distance communication.

Additional video broadcasting experiments are conducted based on the characterization experiments. From this experiment, it can be confirmed that the video stopped and replayed in accordance with the operation of the IRS.

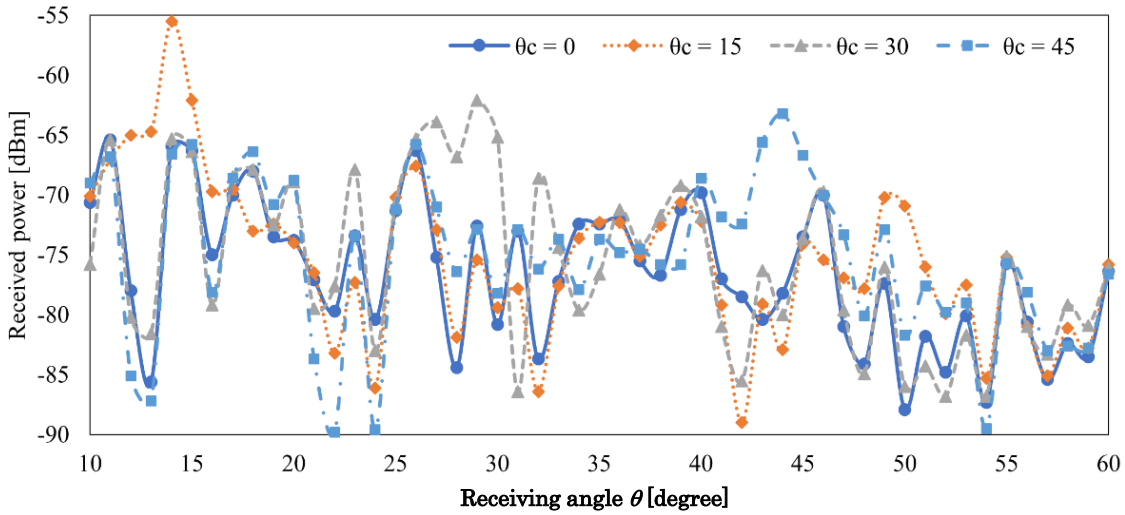

Fig. VIII-8. Experimental results.

VIII-4. Conclusion

In this paper, we introduce the outline of the prototype IRS for 60 GHz band, the analyzed results by the EM simulation, and the results of characterization experiments. The development process and the experimental results show the effectiveness of the IRS as a device for improving the propagation path, and also reveal some issues, including

the expansion of operating bandwidth, the reduction of beam squint, and the manufacturing cost. In the future, it will be necessary to consider the desirable equipment configuration for B5G/6G.

REFERENCE

[1] Beyond 5G Promotion Strategy (Outline) (MIC, in Japanese) https://www.soumu.go.jp/main_content/000702111.pdf

[2] R. Hibi, Y. Kawamoto and N. Kato, "Standalone-Intelligent Reflecting Surface Control Method Using Hierarchical Exploration by Beamwidth Expansion and Environment-Adaptive Codebook," in IEEE Transactions on Vehicular Technology, vol. 72, no. 9, pp. 11990-12000, Sept. 2023.

[3] H. Hashida, Y. Kawamoto, and N. Kato, "Selective Reflection Control: Distributed IRS-Aided Communication with Partial Channel State Information," IEEE Transactions on Vehicular Technology, vol. 71, no. 11, pp. 11949-11958, Nov. 2022.

[4] D. Kitayama, D. Kurita, K. Miyachi, S. Itoh, and T. Tachizawa, "5G radio access experiments on coverage expansion using metasurface reflector at 28 GHz," 2019 IEEE Asia-pacific microwave conference (APMC), pp. 435-437, Dec. 2019.

[5] L. Dai, B. Wang, M. Wang, X. Yang, et al., "Reconfigurable intelligent surface-based wireless communications: antenna design, prototyping and experimental results," IEEE access, vol. B, pp. 45913-45923, March 2020.

[6] A. Couch and A. Grbic, "A phase-tunable, liquid crystal-based metasurface," 10th International Congress on Advanced Electromagnetic Materials in Microwaves and Optics-metamaterials, pp. 94-96, Sept. 2016.

[7] Press release of Tohoku university, May 2023. (in Japanese) tohokuuniv_press0524_01web_60ghz.pdf

IX. Wireless Transport Technology for Xhaul

Hiroaki Asano Panasonic System Networks R&D Lab.
Takeshi Yasunaga Panasonic Connect

Abstract— **This paper provides an overview of wireless transport technology for xhaul and describes the points that unlicensed bands are expected to be actively used in 6G networks. Next, we describe the developed wireless transport equipment using 60 GHz unlicensed bands and future trends. And, for mobility platforms using 60GHz, the developed technology that uses millimeter wave radar with machine learning to predict wireless quality to avoid blocking and achieve seamless handover and RAT change is also described. These technologies are expected to expand to wireless transport technology for xhaul.**

IX-1. Introduction

In 5G networks, configuration in which CUs, DUs, and RUs are prepared according to RAN function split option 2 and option 7-2 and are connected via backhaul, midhaul, and fronthaul are often used. In addition to large capacity, flexibility, scalability, power saving, low cost, reliability, security, and integrated management are required for RAN, and is being put into practical use for 5G [1]. For 6G networks, RAN functional splitting, virtualization and various functions have been considered according to requirements [2]. Support for NTN will be required, and traffic per user will further increase, user density will also increase, and higher frequency bands will be used for access networks. With the study of cell-free technology or distributed MIMO, it is necessary to place many antennas close to terminals. It is also required that antennas will be mounted on UAVs, HAPSs or LEO/GEOs, and it can be used in areas where conventional service coverage is difficult, and it is also desirable to support moving cells such as vehicles or high-speed trains. In these cases, wireless transport technology for xhaul will become more important. Fig. IX-1 shows RAN architecture with xhaul.

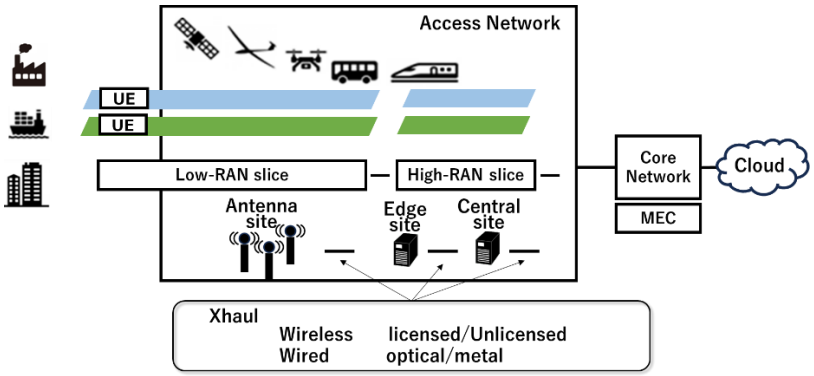

Fig. IX-1. RAN architecture and xhaul technology.

Regarding wireless, it is desirable to actively utilize unlicensed bands in addition to licensed bands. Discussions regarding frequency allocation in licensed bands will continue, in addition to this, effective use of unlicensed bands will enable the early realization of 6G networks.

When using an unlicensed band, sufficient management is required to prevent unexpected interference when sharing it with other users. The RAN is required to comprehensively manage the operational status of xhaul, including the use of unlicensed bands, and to realize efficient operation of the entire network.

IX-2. Unlicensed Band Technology for Wireless Transport

In 6G networks, it is expected that unlicensed bands will be used for wireless transport for xhaul. Here, the IEEE802.11ad [3] compliant wireless equipment and the system technology that uses the unlicensed 60GHz band, which has the potential to be used for wireless transport for xhaul, are described.

IX-2.1. 60GHz Wireless Transport Equipment (IEEE802.11ad)

We have developed the 60GHz band wireless transmission equipment that was compliant with IEEE802.11ad. The equipment has the beamforming function using the 32-element antenna, and autonomously select the optimal beam for communication between an AP and STAs within a ±60° range. Devices equipped with lens antennas are also prepared.

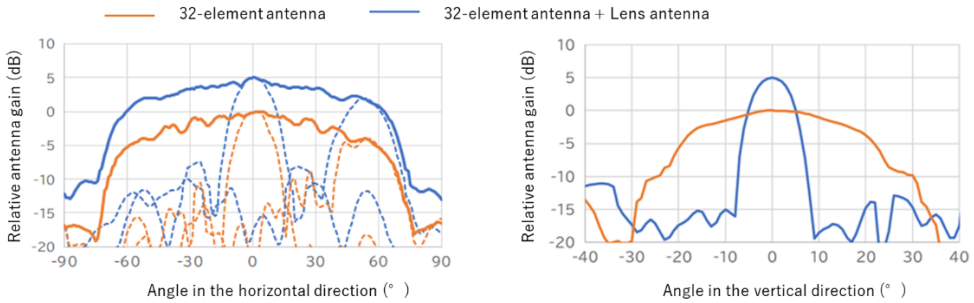

Fig. IX-2. The horizontal and vertical antenna gain with/without the lens antenna.

Lens antennas ensure antenna gain by narrowing the beam width in the vertical direction and enable long-distance transmission. The horizontal and vertical antenna gains with and without the lens antenna are shown in Fig. IX-2 By using the lens antenna, the beam is narrowed in the vertical direction, and beamforming remains unchanged in the horizontal direction. Fig. IX-3 shows the results of evaluating the transmission throughput at the IP layer with respect to the distance/wireless quality between the AP and the STA. The equipment implements up to MCS12, and the

theoretical value at the IP layer for each MCS value is also shown in dotted lines. The evaluation result shows that communication is possible at over 2.5Gbps up to about 120m, and transmission speeds of about 1Gbps can be obtained up to about 300m. This is the result of evaluation using devices equipped with lens antennas.

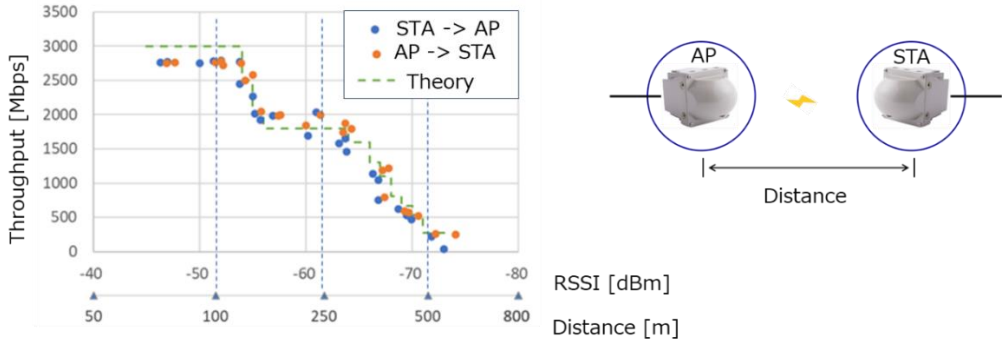

Fig. IX-3. The transmission evaluation results of the wireless transport device

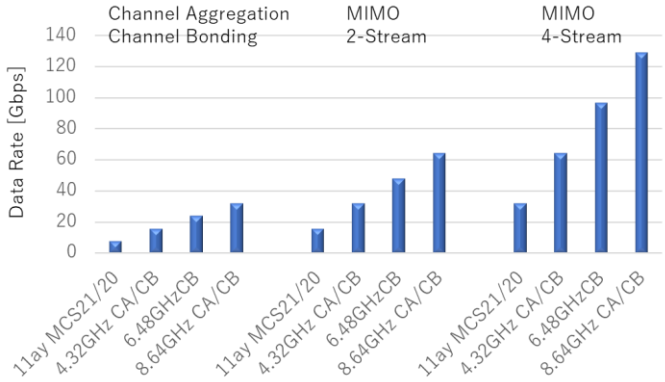

Fig. IX-4. Data rates at PHY layer specified in IEEE802.11ay

Fig. IX-4 shows the transmission rate at PHY layer specified by IEEE802.11ay [4], which was specified further advancement of IEEE802.11ad. In Japan, up to four channels are available at 2.16GHz per channel from 57GHz to 66GHz. In IEEE802.11ay, when using four channels simultaneously with channel aggregation or channel bonding, the maximum transmission speeds on the physical layer are 64.7Gb/s with 2-Stream MIMO and 129.4Gb/s with 4-Stream MIMO. It has plenty of potential to support increased capacity for 6G networks.

IX-2.2. Wireless Transport for Mobility Platform

Millimeter wave transmission is required to be utilized for mobility platforms to achieve large capacity, for example, to support moving cells. Millimeter-wave transmission is highly susceptible to shielding due to its linearity, so techniques to predict and avoid shielding are needed. To solve this problem, we have developed the

technology to predict wireless quality using millimeter wave radar and machine learning. Fig. IX-5 shows the developed millimeter wave transport system for mobility platform using 5G-GWs. The 5G-GW was equipped with the AP and the STA of 60 GHz W-LAN (Wireless LAN) for multi-hop backhaul, and the AP to provide the 60 GHz W-LAN access network for vehicles, and the sensor using 79 GHz millimeter wave radar. When a terminal enters a shielded area or moves through an area where millimeter-wave radio quality is degraded, it realizes the function that connects to the optimal RAT or neighboring millimeter-wave AP based on the radio quality prediction.

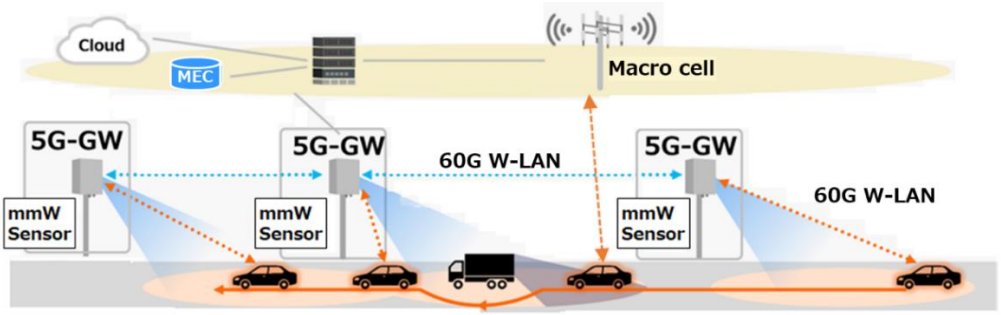

Fig. IX-5. Millimeter wave transport system for mobility platform

Fig. IX-6 shows the developed mechanism to prepare radio quality maps from point cloud data which is acquired by the millimeter wave radar. Extracting vehicle information from millimeter-wave radar point cloud data using machine learning is the first step. The second step is predicting vehicle positions based on the extracted vehicle information with corrections using lane and inter-vehicle distance information. And the third is generating a dynamic radio quality map for use in prediction based on the predicted vehicle positions [5].

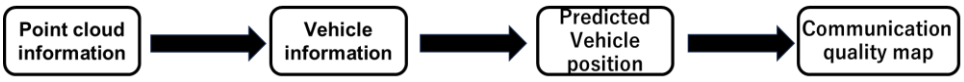

Fig. IX-6. The developed mechanism to prepare radio quality maps from point cloud data which is acquired by the millimeter wave radar.

Using the developed mechanism, we developed the evaluation system and verified that performs RAT switching from 60 GHz W-LAN to Macro Cell when shielding was expected to occur, and handover to millimeter wave cells at adjacent 5G-GWs in a course where multiple 5G-GWs were placed adjacent to each other. Fig. IX-7 shows the evaluation system.

Fig. IX-8 shows the throughput evaluation results of video stream transmission from the vehicle with and without radio quality prediction when the vehicle was moving [6]. The handover and RAT switching could be performed seamlessly when the radio quality

was predicted. This is an example of a technology using unlicensed band that enables millimeter wave transmission to support mobility platforms.

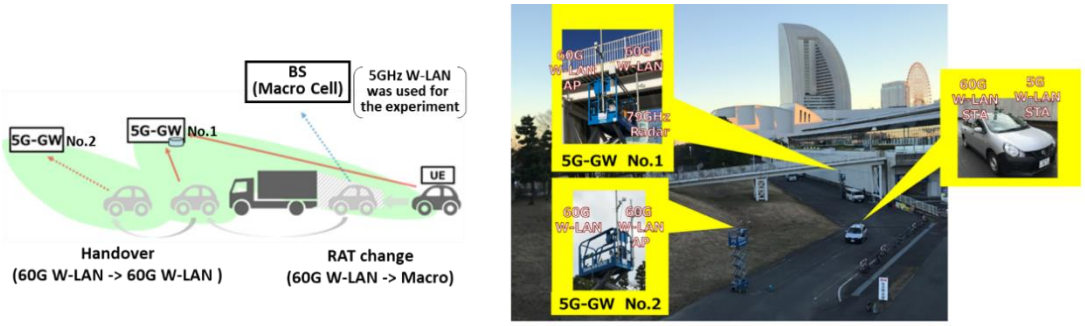

Fig. IX-7. The evaluation system

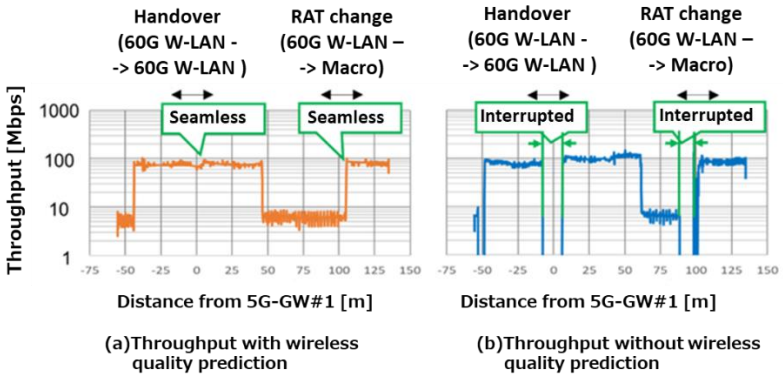

Fig. IX-8. The results of the throughput with/without wireless quality prediction

IX-3. Conclusion

In this paper, we explained the importance of wireless transport technology for xhaul and the direction in which unlicensed bands will be used in 6G networks. And the developed unlicensed 60 GHz W-LAN equipment which is compliant to IEEE802.11ad and its application to a mobility platform that can avoid blocking and realize seamless RAT change and handover by using millimeter wave sensors with machine learning to predict radio quality were described. These technologies are expected to expand to wireless transport technology for xhaul.

Acknowledgements

Some part of this paper was supported by “Research and development project for expansion of radio spectrum resources” of MIC, Japan. (JPJ000254)

REFERENCE

[1] Y. Yoshida," Mobile Xhaul Evolution: Enabling Tools for a Flexible 5G Xhaul Network," OFC, 2018

[2] N. Aihara, et. al.," A User-Centric RAN Architecture using Cell Free massive-MIMO for 6G System," 2021 IEICE Society conference BS-3-9, Sep. 2021.

[3] IEEE, "802.11ad-2012 – IEEE standard for local and metropolitan area networks – Part 11: Wireless LAN Medium Access Control (MAC) and Physical Layer (PHY) Specifications Amendment 3: Enhancements for Very High Throughput in the 60 GHz Band," Dec. 2012

[4] IEEE, "802.11ay-2021 - IEEE Standard for Information Technology--Telecommunications and Information Exchange between Systems Local and Metropolitan Area Networks--Specific Requirements Part 11: Wireless LAN Medium Access Control (MAC) and Physical Layer (PHY) Specifications Amendment 2: Enhanced Throughput for Operation in License-exempt Bands above 45 GHz," Jul. 2021.

[5] H.Asano, et al., "High power efficiency millimeter-wave network with communication quality prediction technology," IEEE VTS 17th APWCS, 2021.

[6] M.Uesugi, et al., "A Study of Uninterrupted Handover Scheme between Millimeter Waves for 5G Advanced System," 2023 IEICE General conference B-5-97, Mar. 2023.

X. A Study on High-Capacity UL Communication in Relay Systems with UAV

Kazuyuki Ozaki, Shunsuke Fujio, Kazuo Shirakawa,
Fujitsu Limited

Abstract— In a mobile radio communication system using high frequency bands such as millimeter wave band and quasi-terahertz band capable of securing wide band, since communication performance of uplink deteriorates in comparison with that of downlink, asymmetry of UL and DL communication performance becomes a problem. The authors think that the communication performance of the uplink can be improved by mounting a relay communication terminal on a device such as UAV (Unmanned Aerial Vehicle) and controlling it in a place where a line of sight (LOS) can be secured between a user terminal and a base station and between the base station and the relay communication terminal. On the other hand, if the relay communication terminal mounted on the UAV cannot be controlled to the optimum position, the improvement effect decreases. In addition, since the distance between the relay communication terminal mounted on the UAV and the base station differs depending on the position of the UAV, the propagation environment changes greatly. Therefore, in this paper, we proposed a method to control relay communication terminals at a place capable of maximizing up-link system capacity, and asymmetric LOS-MIMO with different antenna construction by robust transmission and reception to change of propagation environment, to show computer simulation results.

X-1. Introduction

For Beyond 5G/6G, further realization of large capacity and high-speed transmission is required, and utilization of high frequency band such as millimeter wave and quasi-terahertz band which can secure wide band is important [1]. However, the degradation of the transmission capacity of the uplink caused by the inability to raise the effective radiated power of the user terminal (UE) becomes a factor inhibiting the promotion of the utilization of the high frequency band. Therefore, to improve the transmission capacity of the uplink, the authors are examining a mobile relay communication system in which a relay communication terminal (RS: Relay Station) is mounted on a UAV (Unmanned Aerial Vehicle), etc., and the RS moves with the movement of the UE. Though the application of the spatial multiplexing technology is effective in the communication between RS and UE for the transmission capacity improvement, there is a concern that the transmission capacity cannot be sufficiently improved because interference occurs between UEs to be multiplexed depending on the positional relation between RS and UE. Since the communication between the UAV and the base station

(BS) becomes LOS and the distance between the UAV and the BS is different according to the movement of the UAV, the LOS-MIMO technology which is robust for the propagation environment is necessary. In this paper, we propose an optimal placement method of a relay communication terminal mounted on a UAV and asymmetric LOS-MIMO technology with different antenna configurations for transmission and reception.

X-2. Proposed Placement Method

In this paper, we assume a system in which an RS capable of forming multiple beams performs uplink communication by MU-MIMO (Multiuser MIMO) with different selected beams. By determining the arrangement (position and orientation of the antenna) of a plurality of RSs according to the position of the UE and considering the number of spatial multiplexes, high efficiency of spatial multiplexing by RS is attempted. The outline of the study system is shown in Fig. X-1.

Considering that the place where the RS can be arranged is limited by the actual environment, the arrangement of each RS is selected from the predetermined arrangement candidates. However, since the communication quality between the BS and RS is also important for relay communication, it is assumed that placement candidates whose sufficient quality cannot be obtained are excluded. In order of one RS each, the spatial multiplicity in each configuration candidate, that is, the number of different selected beams, is estimated and the configuration with the largest spatial multiplicity is determined. However, if there are multiple configurations with the maximum number of multiplexes, the configuration with the maximum transmission capacity is selected. This is repeated sequentially for all RSs to determine the placement of all RSs. It is assumed that the multiplicity and transmission capacity in each placement candidate are calculated by simply estimating the propagation path based on the positional relationship between RS and UE. However, in this paper, as an initial examination, the position information of BS, RS, UE, and each propagation path information are all known.

The characteristics with our proposed optimal placement method are evaluated by computer simulation. Assuming a scenario in which three RSs cover the cell edge area of a BS sector with a three-sector configuration, the transmission capacity of the uplink was evaluated. In this evaluation, only the communication from UE to RS was considered, and the communication with the BS was ignored. All propagation paths are visible and only one direct wave path is considered. Each UE selects and connects the RS and the beam with the maximum received power. The user scheduling of RS assumes round-robin and selects the connection UE with different selection beams up to the maximum space multiplex number and carries out the communication. The RS configuration was compared between the case in which the RS configuration was evenly spaced at 30 m

above the BS at a distance of 80 m and the case in which the RS configuration was determined by the proposed method according to the UE position from the grid points in 5 m increments. The maximum spatial multiplicity of RS is set to 4, and MMSE is assumed for signal separation.

Fig. X-2 shows the transmission capacity characteristics with respect to the number of UEs. Since the possibility of spatial multiplexing of many UEs increases as the number of UEs increases, the transmission capacity also increases with the increase in the number of UEs in any arrangement. However, as mentioned above, by deciding the arrangement by the optimal arrangement method, even when the number of UEs is small, many spatial multiplexes can be utilized, and therefore, a high value of the transmission capacity is obtained. Compared with the case where the arrangement is fixed, 13% of 24UE and 27% of 12UE can be confirmed to improve the transmission capacity.

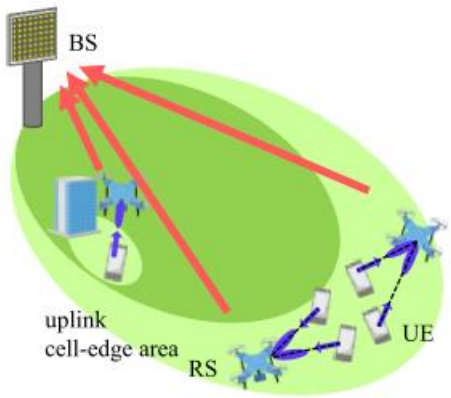

Fig. X-1. Illustration of the UAV-assisted cellular network system

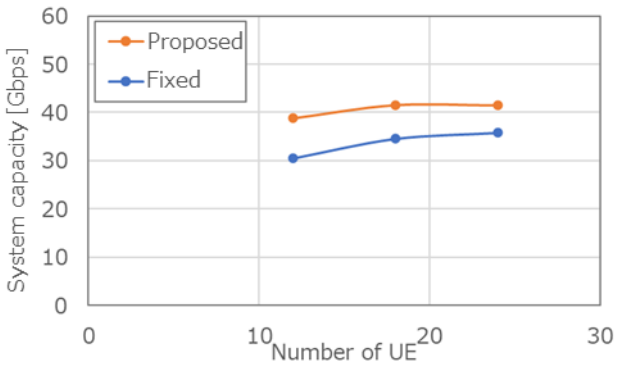

Fig. X-2. System capacity performance

X-3. Robust LOS-MIMO

As described in Chapter 2, this paper assumes LOS between RS and BS, so direct wave dominates as the propagation environment. Therefore, in Backhaul communication

between RS and BS, it is impossible to apply MIMO technology using multipath which is generally used in mobile radio communication systems, so technology to improve transmission speed is required. Hence, we consider applying LOS-MIMO to backhaul links. In Symmetric-LOS-MIMO (SLOS-MIMO) with the same antenna configuration for transmission and reception, the propagation channel between transmission and reception is uniquely determined by the distance between transmission and reception and the element spacing of the antenna. Even if excellent performance is obtained at a certain distance between transmission and reception, it is known that the robustness to the distance between transmission and reception is poor because the performance deteriorates significantly when the distance between transmission and reception changes [2]. Therefore, SLOS-MIMO is difficult to apply to RS, and we assume asymmetric LOS-MIMO (Asymmetric LOS-MIMO: ALOS-MIMO) with different antenna configurations for transmission and reception, as discussed in [2]. As revealed in, asymmetric LOS-MIMO shows less degradation of channel capacity for transmit/receive distance and more robustness for transmit/receive distance than symmetric LOS-MIMO.

Although simulation results and experimental results are shown when antennas are placed on the circumference of a certain plane and are opposed to each other, no study has been made on Uniform Linear Array (ULA) or Uniform Rectangular Array (URA) adopted in BSs such as 5G. In this paper, we investigate asymmetric LOS-MIMO when ULA and URA antenna configurations are adopted.

The antenna for transmission and reception is constructed on a certain plane, and the case in which the planes face each other so as to be parallel is assumed. All propagation paths are visible and only one direct wave path is considered. The antenna element spacing for transmission and reception was calculated using R=20 m by using ideal equation [3] for ULA and URA.

Fig. X-3 (a) shows the channel capacities of symmetric LOS-MIMO (SLOS-MIMO) and asymmetric LOS-MIMO (Asymmetric LOS-MIMO (ALOS-MIMO)) in ULA. As can be seen from the figure, SLOS-MIMO shows a drop in channel capacity around 10 and 15 m, while ALOS-MIMO shows no drop in channel capacity after 8 m. Fig. X-3 (b) shows the channel capacities of SLOS-MIMO and ALOS-MIMO in the URA. Like ULA, SLOS-MIMO shows a drop in channel capacity around 10 m, while ALOS-MIMO shows no drop after 10 m.

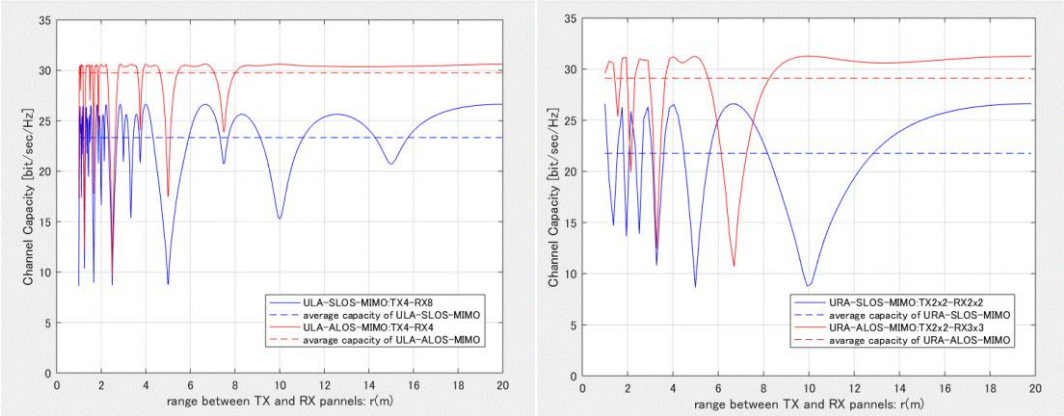

(a) ULA (b) URA

Fig. X-3. Channel capacity performance of ALOS-MIMO and SLOS-MIMO

X-4. Conclusion

In this paper, we discuss the optimal placement method of RS considering the multiplicity of UE accommodations and the robust LOS-MIMO for robust capacity enhancement between RS and BS in high frequency mobile radio communication systems using mobile relay communication terminal such as UAV. Computer simulation results show that the optimal placement method can achieve 27% of maximum transmission capacity, and robust LOS-MIMO to increase the capacity of RS and BS.

Acknowledgements

This research is supported by the Ministry of Internal Affairs and Communications in Japan (JPJ000254).

REFERENCE

[1] 3GPP TS 38.104 V15.0.0, “Base Station (BS) radio transmission and reception,” Dec. 2017.

[2] N. Matsumura, K. Nishimori, R. Taniguchi, T. Hiraguri, T. Tomura and J. Hirokawa, "Novel Unmanned Aerial Vehicle-Based Line-of-Sight MIMO Configuration Independent of Transmitted Distance Using Millimeter Wave," IEEE Access, Vol. 8, pp. 11679-11691, 2020.

[3] Bøhagen, F., Orten, P. & Øien, G. Optimal Design of Uniform Rectangular Antenna Arrays for Strong Line-of-Sight MIMO Channels. J Wireless Com Network 2007, 045084

Abbreviation List

Abbreviation	Explanation
ABG	Alpha-Beta-Gamma
AI	Artificial Intelligence
ALD	Atomic Layer Deposited
AMC	Adaptive Modulation and Coding
AoA	Angle of Arrival
AR	Augmented Reality
ASIC	Application Specific Integrated Circuit
AWG	Arbitrary Waveform Generator
BAN	Body Area Network
BCB	Benzo cyclobutene
BER	Bit Error Rate
BF	BeamForming
BS	Base Station
CC	Component Carrier
CI	Close-in
CMOS	Complementary Metal Oxide Semiconductor
CPS	Cyber Physical System
CSI	Channel State Information
DC	Direct Current
DFT	Discrete Fourier Transform
DL	Down Link
DNN	Deep Neural Network
DOA	Direction of Arrival
DSP	Digital Signal Processing
EIRP	
EVM	Error Vector Magnitude
eWLB	embedded Wafer Level Ball grid array
FDD	Frequency Division Duplex
FDE	Frequency Domain Equalize

Abbreviation	Explanation
FSPL	Free Space Path Loss
HARQ	Hybrid Automatic Repeat Request
HPBW	Half Power Beam Width
IBO	Input Back Off
IFFT	Inverse Fast Fourier Transform
InH	Indoor hotspot cell
ISAC	Integrated Sensing and Communication
ITU-R	International Telecommunication Union Radiocommunication Sector
KPI	Key Performance Indicator
LAN	Local Area Network
LNA	Low-Noise Amplifier
LOS	Light of Sight
LTE	Long Tern Evolution
MCM	Multichip Module
MIMO	Multiple-Input and Multiple-Output
MMIC	Monolithic Microwave IC
MS	Mobile Station
MOS	Metal Oxide Semiconductor
MOS-HEMT	Metal-Oxide-Semiconductor Eigh-Electron-Mobility Transistor
MSL	Microstrip Line
NLOS	Non-Line of Sight
NR	New Radio
NRNT	New Radio Network Topology
OAM	Orbital Angular Momentum
OFDM	Orthogonal Frequency Division Multiplexing
PA	Power Amplifier
PAE	
PCB	Printed Circuit Board
PLE	Path Loss Exponent
QMH	Qualitative Microwave Holography
RAN	Radio Access Network

Abbreviation	Explanation
RAT	Radio Access Technology
RD	Relay Device
RF	Radio Frequency
RIS	Reconfigurable Intelligent Surface
RMSE	Root Mean Square Error
RS	Relay Station
Rx	Receiver
SAG	Selective-Area Growth
SC	Single Carrier
SiP	System-in-Package
SISO	Single-Input Single-Output
SIW	Substrate-Integrated Waveguide
SNR	Signal to Noise power Ratio
TDD	Time Division Duplex
TDS	Time Domain Spectroscopy
THz	Tera Hertz
TMA	Trimethylaluminum
TSV	Through-silicon Via
Tx	Transmitter
UCA	Uniform Circular Array
UE	User Equipment
UL	Up Link
VR	Virtual Reality